15 Conceptual Models and Computer Models

Horst D. Schulz

Upon recording *processes* of nature quantitatively, the term model is closely related to the term system. A *system* is a segment derived from nature with either real or, at least, imagined boundaries. Within these boundaries, there are processes which are to be analyzed. Outside, there is the *environment* exerting an influence on the course of the procedural events which are internal to the system by means of the *boundary conditions*. A *conceptual model* contains principle statements, mostly translatable quantitatively, with regard to the processes in a system and the influence of prevalent boundary conditions. If the systems to be reproduced are especially complex, any significant realization of the conceptual model is often only possible by applying computer models.

Depending on the field of interest and the nature of the task, the processes in a model will be either somewhat more physical/hydraulic, geochemical, biogeochemical, or biological. The systems and processes studied might then expand in size over the great oceans and their extensive stream patterns down to small segments of deep ocean floor measuring only few cubic centimeters, including the communities of microorganisms living therein. Consequently, there are no predefined dimensions or structures which are valid for the systems and their models, instead, these are exclusively determined by the understanding of the respective processes of interest and their quantitative translatability. Since geochemical and biogeochemical reactions occur relatively fast, and are thus bound to spaces of smaller dimensions, the models dealt with in this chapter will be preferentially concerned with dimensions encompassing few centimeters and meters of sediment, to some hundred meters of water column.

In the field of applied geological sciences, models frequently assume a primarily prognostic character. For instance, after accomplishing an adequate calibration, an hydraulic model applied to groundwater, or a model of solute transport in groundwater, is primarily supposed to predict the system's reaction as precisely as possible under the given boundary conditions. Such models will find very practical and often well paid applications. In marine geochemistry such a prognostic function of models occurs rather seldom; here, the objective of obtaining a quantitative concept of a system predominates in most cases, which is 'function' of a particular segment of nature. Computer models can then check the plausibility of model concepts of complex systems, can draw attention to the areas not sufficiently understood, and might help discover parameters with which the system can be described reasonably well and effectively.

In the following, zero-dimensional geochemical reaction models will be distinguished from one-dimensional models, in which transport processes are coupled by various means to geochemical and biogeochemical reactions. The subsections will then introduce approaches to very different models, including models that have advanced to very different stages of development.

15.1 Geochemical Models

15.1.1 Structure of Geochemical Models

Zero-dimensional geochemical models are concerned with the contents of solutions of an aquatic subsystem (e.g. pore water, ocean water, precipitation, groundwater), the equilibria between the various dissolved species as well as their adjoining gaseous and solid phases. A computer model by the name of WATEQ (derived from water-equilibria) was published for the first time by Truesdell and Jones (1974). Unfortunately, this was done in the computer language PL1 which has

become completely forgotten by now. Afterwards a FORTRAN version had followed (WATEQF) released by Plummer et al. (1976) as well as another revised version (WATEQ4F) by Ball and Nordstrom (1991).

All these programs share the common feature that they start out from water analyses which were designed as comprehensive as possible, along with conceiving the measured values as cumulative parameters (sums of all aquatic species), only to subsequently allocate them to the various aquatic species. This was done by applying iteration calculus that accounts for the equilibria related to the various aquatic species.

For instance, the measured value of calcium in an ocean water sample containing 10.6 mmoles/l is allocated to 9.51 mmol/l Ca^{2+}, 1.08 mmol/l $CaSO_4^0$, 0.04 mmol/l $CaHCO_3^+$, and to a series of low concentrated other calcium species in solution. The analysis of sulfate yielding 29.26 mmol/l is allocated accordingly to 14.67 mmol/l SO_4^{2-}, 7.30 mmol/l $NaSO_4^-$, 1.08 mmol/l $CaSO_4^0$, 0.16 mmol/l KSO_4^-, and, likewise, to a number of low concentrated sulfate species. The procedure is similarly applied to all analytical values. Table 15.2 summarizes the species allocations for the ocean water analysis previously shown in Table 15.1.

Table 15.1 This ocean water analysis carried out by Nordstrom et al. (1979) has been frequently used to test and compare various geochemical model programs.

Seawater from Nordstrom et al. (1979)		
pH	=	8.22
pe	=	8.451
Ionic strength	=	6.750E-1
Temperature (°C)	=	25.0
Elements		*Molality*
Alkalinity		2.406E-3
Ca		1.066E-2
Cl		5.657E-1
Fe		3.711E-8
K		1.058E-2
Mg		5.507E-2
Mn		3.773E-9
N (-III)		1.724E-6
N (V)		4.847E-6
Na		4.854E-1
O (0)		3.746E-4
S (VI)		2.926E-2
Si		7.382E-5

Based on the activities of the non-complex aquatic species (e.g. $[Ca^{2+}]$ or $[SO_4^{2-}]$, the next step consists in calculating the saturation indices (SI) of each compound mineral:

$$SI = \log\left(IAP \Big/ K_{sp} \right) \tag{15.1}$$

In this equation IAP denotes the Ion Activity Product (in the example of gypsum or anhydrite these would be $([Ca^{2+}]\cdot[SO_4^{2-}])$. K_{SP} is the solubility product constant of the respective mineral. A saturation index SI = 0 describes the condition in which the solution of the corresponding mineral is just saturated, SI > 0 describes the condition of supersaturation of the solution, SI < 0 its undersaturation. The activity [A] of a substance is calculated according to the equation:

$$[A] = (A) \cdot \gamma_A \tag{15.2}$$

Here, (A) is the concentration of a substance measured in moles/l and γ_A is the activity coefficient calculated as a function of the overall ionic strength in the solution. For infinitesimal diluted solutions, the activity coefficients assume the value of 1; hence, activity equals concentration. In ocean water, the various monovalent ions, or ion pairs, display activity coefficients somewhere around 0.75; whereas the various divalent ions, or ion pairs, display values around 0.2 (cf. Table 15.2, last column).

After transformation, the equation 15.1 to calculate the saturation index of the mineral gypsum reads:

$$SI_{gypsum} = \log\left(\frac{[Ca^{2+}] \cdot [SO_4^{2-}]}{K_{sp,gypsum}} \right) \tag{15.3}$$

If we now insert the solubility product constant for gypsum $K_{sp,gypsum} = 2.63 \cdot 10^{-5}$ in the equation and the exemplary values mentioned above for ocean water (activity coefficients of divalent ions ≈ 0.2; concentration of Ca^{2+} = 9.15/1000 mol/l;

Table 15.2 For an analysis of Table 15.1, this allocation of the aquatic species was calculated with the geochemical model program PHREEQC.

	Species	Molality	Activity	Molality log	Activity log	Gamma log
	OH^-	2.18E-06	1.63E-06	-5.661	-5.788	-0.127
	H^+	7.99E-09	6.03E-09	-8.098	-8.220	-0.122
	H_2O	5.55E+01	9.81E-01	-0.009	-0.009	0.000
C (IV)		2.181E-03				
	HCO_3^-	1.52E-03	1.03E-03	-2.819	-2.989	-0.171
	$MgHCO_3^+$	2.20E-04	1.64E-04	-3.659	-3.785	-0.127
	$NaHCO_3$	1.67E-04	1.95E-04	-3.778	-3.710	0.068
	$MgCO_3$	8.90E-05	1.04E-04	-4.050	-3.983	0.068
	$NaCO_3^-$	6.73E-05	5.03E-05	-4.172	-4.299	-0.127
	$CaHCO_3^+$	4.16E-05	3.10E-05	-4.381	-4.508	-0.127
	CO_3^{-2}	3.84E-05	7.98E-06	-4.415	-5.098	-0.683
	$CaCO_3$	2.72E-05	3.17E-05	-4.566	-4.499	0.068
	CO_2	1.21E-05	1.42E-05	-4.916	-4.849	0.068
	$MnCO_3$	3.18E-10	3.71E-10	-9.498	-9.430	0.068
	$MnHCO_3^+$	7.17E-11	5.36E-11	-10.144	-10.271	-0.127
	$FeCO_3$	1.96E-20	2.29E-20	-19.709	-19.641	0.068
	$FeHCO_3^+$	1.64E-20	1.22E-20	-19.785	-19.912	-0.127
Ca		1.066E-02				
	Ca^{+2}	9.51E-03	2.37E-03	-2.022	-2.625	-0.603
	$CaSO_4$	1.08E-03	1.26E-03	-2.967	-2.900	0.068
	$CaHCO_3^+$	4.16E-05	3.10E-05	-4.381	-4.508	-0.127
	$CaCO_3$	2.72E-05	3.17E-05	-4.566	-4.499	0.068
	$CaOH^+$	8.59E-08	6.41E-08	-7.066	-7.193	-0.127
	$CaHSO_4^+$	5.96E-11	4.45E-11	-10.225	-10.352	-0.127
Cl		5.656E-01				
	Cl^-	5.66E-01	3.52E-01	-0.247	-0.453	-0.206
	$MnCl^+$	1.13E-09	8.41E-10	-8.948	-9.075	-0.127
	$MnCl_2$	1.11E-10	1.29E-10	-9.956	-9.888	0.068
	$MnCl_3^-$	1.68E-11	1.26E-11	-10.774	-10.901	-0.127
	$FeCl^{+2}$	9.58E-19	2.97E-19	-18.019	-18.527	-0.508
	$FeCl_2^+$	6.27E-19	4.68E-19	-18.203	-18.330	-0.127
	$FeCl^+$	7.78E-20	5.81E-20	-19.109	-19.236	-0.127
	$FeCl_3$	1.41E-20	1.65E-20	-19.850	-19.783	0.068
Fe (II)		5.550E-19				
	Fe^{+2}	3.85E-19	1.19E-19	-18.415	-18.923	-0.508
	$FeCl^+$	7.78E-20	5.81E-20	-19.109	-19.236	-0.127
	$FeSO_4$	4.84E-20	5.65E-20	-19.315	-19.248	0.068
	$FeCO_3$	1.96E-20	2.29E-20	-19.709	-19.641	0.068
	$FeHCO_3^+$	1.64E-20	1.22E-20	-19.785	-19.912	-0.127
	$FeOH^+$	8.23E-21	6.15E-21	-20.084	-20.211	-0.127
Fe (III)		3.711E-08				
	$Fe(OH)_3$	2.84E-08	3.32E-08	-7.547	-7.479	0.068
	$Fe(OH)_4^-$	6.60E-09	4.92E-09	-8.181	-8.308	-0.127
	$Fe(OH)_2^+$	2.12E-09	1.58E-09	-8.674	-8.801	-0.127
	$FeOH^{+2}$	9.46E-14	2.94E-14	-13.024	-13.532	-0.508
	$FeSO_4^+$	1.09E-18	8.16E-19	-17.962	-18.089	-0.127
	$FeCl^{+2}$	9.58E-19	2.97E-19	-18.019	-18.527	-0.508
	$FeCl_2^+$	6.27E-19	4.68E-19	-18.203	-18.330	-0.127
	Fe^{+3}	3.88E-19	2.80E-20	-18.411	-19.554	-1.143
	$Fe(SO_4)_2^-$	6.36E-20	4.75E-20	-19.196	-19.323	-0.127
	$FeCl_3$	1.41E-20	1.65E-20	-19.850	-19.783	0.068
K		1.058E-02				
	K^+	1.04E-02	6.49E-03	-1.982	-2.188	-0.206
	KSO_4^-	1.64E-04	1.22E-04	-3.786	-3.913	-0.127

Table 15.2 continued.

	Species	Molality	Activity	Molality log	Activity log	Gamma log
Mg		5.507E-02				
	Mg^{+2}	4.75E-02	1.37E-02	-1.324	-1.864	-0.541
	$MgSO_4$	7.30E-03	8.53E-03	-2.137	-2.069	0.068
	$MgHCO_3^+$	2.20E-04	1.64E-04	-3.659	-3.785	-0.127
	$MgCO_3$	8.90E-05	1.04E-04	-4.050	-3.983	0.068
	$MgOH^+$	1.08E-05	8.07E-06	-4.966	-5.093	-0.127
Mn (II)		3.773E-09				
	Mn^{+2}	1.89E-09	5.86E-10	-8.724	-9.232	-0.508
	$MnCl^+$	1.13E-09	8.41E-10	-8.948	-9.075	-0.127
	$MnCO_3$	3.18E-10	3.71E-10	-9.498	-9.430	0.068
	$MnSO_4$	2.38E-10	2.77E-10	-9.624	-9.557	0.068
	$MnCl_2$	1.11E-10	1.29E-10	-9.956	-9.888	0.068
	$MnHCO_3^+$	7.17E-11	5.36E-11	-10.144	-10.271	-0.127
	$MnCl_3^-$	1.68E-11	1.26E-11	-10.774	-10.901	-0.127
	$MnOH^+$	3.29E-12	2.45E-12	-11.483	-11.610	-0.127
	$Mn(OH)_3^-$	5.36E-20	4.00E-20	-19.271	-19.398	-0.127
	$Mn(NO_3)_2$	2.62E-20	3.06E-20	-19.582	-19.515	0.068
Mn (III)		7.108E-26				
	Mn^{+3}	7.11E-26	5.12E-27	-25.148	-26.291	-1.143
Mn (VI)		2.322E-28				
	MnO_4^{-2}	2.32E-28	7.21E-29	-27.634	-28.142	-0.508
Mn (VII)		1.127E-29				
	MnO_4^-	1.13E-29	8.41E-30	-28.948	-29.075	-0.127
N (-III)		1.724E-06				
	NH_4^+	1.58E-06	1.18E-06	-5.802	-5.929	-0.127
	NH_3	9.36E-08	1.09E-07	-7.029	-6.961	0.068
	$NH_4SO_4^-$	5.40E-08	4.03E-08	-7.267	-7.394	-0.127
N (V)		4.847E-06				
	NO_3^-	4.85E-06	3.62E-06	-5.315	-5.441	-0.127
	$Mn(NO_3)_2$	2.62E-20	3.06E-20	-19.582	-19.515	0.068
Na		4,854E-01				
	Na^+	4.79E-01	3.38E-01	-0.320	-0.471	-0.151
	$NaSO_4^-$	6.05E-03	4.51E-03	-2.219	-2.346	-0.127
	$NaHCO_3$	1.67E-04	1.95E-04	-3.778	-3.710	0.068
	$NaCO_3^-$	6.73E-05	5.03E-05	-4.172	-4.299	-0.127
O (0)		3.746E-04				
	O_2	1.87E-04	2.19E-04	-3.728	-3.660	0.068
S (VI)		2.926E-02				
	SO_4^{-2}	1.47E-02	2.66E-03	-1.833	-2.575	-0.741
	$MgSO_4$	7.30E-03	8.53E-03	-2.137	-2.069	0.068
	$NaSO_4^-$	6.05E-03	4.51E-03	-2.219	-2.346	-0.127
	$CaSO_4$	1.08E-03	1.26E-03	-2.967	-2.900	0.068
	KSO_4^-	1.64E-04	1.22E-04	-3.786	-3.913	-0.127
	$NH_4SO_4^-$	5.40E-08	4.03E-08	-7.267	-7.394	-0.127
	HSO_4^-	2.09E-09	1.56E-09	-8.680	-8.807	-0.127
	$MnSO_4$	2.38E-10	2.77E-10	-9.624	-9.557	0.068
	$CaHSO_4^+$	5.96E-11	4.45E-11	-10.225	-10.352	-0.127
	$FeSO_4^+$	1.09E-18	8.16E-19	-17.962	-18.089	-0.127
	$Fe(SO_4)_2^-$	6.36E-20	4.75E-20	-19.196	-19.323	-0.127
	$FeSO_4$	4.84E-20	5.65E-20	-19.315	-19.248	0.068
	$FeHSO_4^{+2}$	4.24E-26	1.32E-26	-25.373	-25.881	-0.508
	$FeHSO_4^+$	3.00E-27	2.24E-27	-26.523	-26.650	-0.127
Si		7.382E-05				
	H_4SiO_4	7.11E-05	8.31E-05	-4.148	-4.081	0.068
	$H_3SiO_4^-$	2.72E-06	2.03E-06	-5.565	-5.692	-0.127
	$H_2SiO_4^{-2}$	7.39E-11	2.29E-11	-10.131	-10.639	-0.508

concentration of SO_4^{2-} = 14.67/1000 mol/l), yields the following equation:

$$SI_{gypsum,\ seawater} = \log\left\{\left(0.2\cdot\frac{9.15}{1000}\right)\cdot\left(0.2\cdot\frac{14.67}{1000}\right)\Big/2.63\cdot10^{-5}\right\} = -0.69 \quad (15.4)$$

Matching to Tables 15.1 and 15.2 the saturation indices are demonstrated in Table 15.3, likewise calculated by applying the PHREEQC model (Parkhurst 1995; Parkhurst and Appelo 1999). Here, the majority of the saturation indices have been calculated on the basis of mineral phases, however, there are also gaseous phases denoted as 'CO_2(g)', 'H_2(g)', 'NH_3(g)', 'O_2(g)'. The saturation index stands for the common logarithm of the respective partial pressure. The number of minerals and gases listed in Table 15.3 depends on the fact that calculations can only be performed after all the ions involved have been analyzed, and furthermore, provided that the database file of the program contains the appropriate thermodynamic data.

It needs to be stated clearly that the conditions of saturation thus calculated in the process of water analyses are determined *exclusively* on the basis of the prevalent analytical data and the employed data available on equilibria. A mineral shown to be supersaturated must not immediately, or at a later instance, be precipitated from this solution, but *can* be formed, for example, when other conditions are fulfilled, e.g. such standing in relation to the reaction kinetics. At the same time, a mineral found to be *under*saturated does not have to become dissolved immediately or at a later time - after all, it is possible that this mineral will never come in contact with the solution. The result of such a model calculation should just be understood as the statement that certain minerals can be either dissolved or precipitated. It goes without saying that mostly such minerals are of particular interest that have a calculated saturation index close to zero, because this circumstance often refers to set equilibria and hence to corresponding reactions.

A huge number of such geochemical models are available. Apart from the models belonging to the WATEQ family which are only of interest to science history nowadays, the model SOLMINEQ (Kharaka et al. 1988), although designed for waters in crude oil fields, is essential because it contains a special pressure and temperature corrective for the applied constants which might as well be important in marine environments. Other models make use of a temperature corrective only. Unfortunately, the SOLMINEQ model has not been developed any further nor improved since its first release, so that only a first, somewhat faulty version is now available.

Beside the model EQ 3/6 (Wolery 1993), the model PHREEQE (Parkhurst et al. 1980) and its recent successor PHREEQC (Parkhurst 1995; Parkhurst and Appelo 1999) are geochemical models in the true sense of the word. With these, one cannot just calculate any kind of saturation indices on the basis of a previously conducted analysis, afterwards to be interpreted more or less well by giving some meaning to them, instead, almost any process can be simulated almost without any limitation, after pre-selecting boundary conditions (e.g. exchanges with the gaseous phase and dissolution/precipitation of minerals), or specific processes (e.g. decomposition of organic matter with corresponding amounts of nitrogen and phosphorous, mixing of waters containing different solutes).

The only limitation is one's own knowledge as to the process to be modeled. The program PHREEQC can be obtained from the internet as public domain software, including an elaborate, very informative description and many examples, at:

http://wwwbrr.cr.usgs.gov/projects/GWC_coupled/phreeqc/index.html

The examples presented in the following and in Section 9.2 have been calculated exclusively with the program PHREEQC.

15.1.2 Application Examples of Geochemical Modeling

Determination of Saturation Indices in Pore water, Precipitation of Minerals

Saturation indices were determined with the PHREEQC model for the core which pore water concentration profiles were previously shown in Chapter 3, Figure 3.1. Here, our attention was drawn to the supersaturation of several manganese minerals in various depths, and thus in differing redox environments. Figure 15.1 shows the depth profiles for the saturation indices of the minerals

Table 15.3 According to the species distribution shown in Table 15.2, the PHREEQC model (Parkhurst 1995) was also applied to calculate the saturation indices. Here, 'CO_2 (g)', 'H_2(g)', 'NH_3(g)', 'O_2(g)' do not stand for mineral phases, but for gaseous phases in which the saturation index is obtained as the logarithm of the respective partial pressure.

Phase	SI	log IAP	log KT	
Anhydrite	-0.84	-5.20	-4.36	$CaSO_4$
Aragonite	0.61	-7.72	-8.34	$CaCO_3$
Artinite	-2.03	7.57	9.60	$MgCO_3$:$Mg(OH)_2$:$3H_2O$
Birnessite	4.81	5.37	0.56	MnO_2
Bixbyite	-2.68	47.73	50.41	Mn_2O_3
Brucite	-2.28	14.56	16.84	$Mg(OH)_2$
Calcite	0.76	-7.72	-8.48	$CaCO_3$
Chalcedony	-0.51	-4.06	-3.55	SiO_2
Chrysotile	3.36	35.56	32.20	$Mg_3Si_2O_5(OH)_4$
Clinoenstatite	-0.84	10.50	11.34	$MgSiO_3$
CO_2 (g)	-3.38	-21.53	-18.15	CO_2
Cristobalite	-0.48	-4.06	-3.59	SiO_2
Diopside	0.35	20.25	19.89	$CaMgSi_2O_6$
Dolomite	2.40	-14.69	-17.09	$CaMg(CO_3)_2$
Epsomite	-2.36	-4.50	-2.14	$MgSO_4$:$7H_2O$
$Fe(OH)_{2.7}Cl_{0.3}$	5.52	-6.02	-11.54	$Fe(OH)_{2.7}Cl_{0.3}$
$Fe(OH)_3$ (a)	0.19	-3.42	-3.61	$Fe(OH)_3$
$Fe_3(OH)_8$	-12.56	-9.34	3.22	$Fe_3(OH)_8$
Forsterite	-3.24	25.07	28.31	Mg_2SiO_4
Goethite	6.09	-3.41	-9.50	FeOOH
Greenalite	-36.43	-15.62	20.81	$Fe_3Si_2O_5(OH)_4$
Gypsum	-0.64	-5.22	-4.58	$CaSO_4$:$2H_2O$
H_2 (g)	-41.22	1.82	43.04	H_2
Halite	-2.51	-0.92	1.58	NaCl
Hausmannite	1.78	19.77	17.99	Mn_3O_4
Hematite	14.20	-6.81	-21.01	Fe_2O_3
Huntite	1.36	-28.61	-29.97	$CaMg_3(CO_3)_4$
Hydromagnesite	-4.56	-13.33	-8.76	$Mg_5(CO_3)_4(OH)_2$:$4H_2O$
Jarosite (ss)	-9.88	-43.38	-33.50	$(K_{0.77}Na_{0.03}H_{0.2})Fe_3(SO_4)_2(OH)_6$
Magadiite	-6.44	-20.74	-14.30	$NaSi_7O_{13}(OH)_3$:$3H_2O$
Maghemite	3.80	-6.81	-10.61	Fe_2O_3
Magnesite	1.07	-6.96	-8.03	$MgCO_3$
Magnetite	3.96	-9.30	-13.26	Fe_3O_4
Manganite	2.46	6.28	3.82	MnOOH
Melanterite	-19.35	-21.56	-2.21	$FeSO_4$:$7H_2O$
Mirabilite	-2.49	-3.60	-1.11	Na_2SO_4:$10H_2O$
$Mn_2(SO_4)_3$	-54.60	-9.29	45.31	$Mn_2(SO_4)_3$
$MnCl_2$:$4H_2O$	-12.88	-10.17	2.71	$MnCl_2$:$4H_2O$
$MnSO_4$	-14.48	-11.81	2.67	$MnSO_4$
Nahcolite	-2.91	-13.79	-10.88	$NaHCO_3$

Table 15.3 continued

Phase	SI	log IAP	log KT	
Natron	-4.81	-6.12	-1.31	$Na_2CO_3:10H_2O$
Nesquehonite	-1.37	-6.99	-5.62	$MgCO_3:3H_2O$
NH_3 (g)	-8.73	2.29	11.02	NH_3
Nsutite	5.85	5.37	-0.48	MnO_2
O_2 (g)	-0.70	-3.66	-2.96	O_2
Portlandite	-9.00	13.80	22.80	$Ca(OH)_2$
Pyrochroite	-8.01	7.19	15.20	$Mn(OH)_2$
Pyrolusite	7.03	5.37	-1.66	MnO_2
Quartz	-0.08	-4.06	-3.98	SiO_2
Rhodochrosite	-3.20	-14.33	-11.13	$MnCO_3$
Sepiolite	1.15	16.91	15.76	$Mg_2Si_3O_{7.5}OH:3H_2O$
Siderite	-13.13	-24.02	-10.89	$FeCO_3$
SiO_2 (a)	-1.35	-4.06	-2.71	SiO_2
Talc	6.04	27.44	21.40	$Mg_3Si_4O_{10}(OH)_2$
Thenardite	-3.34	-3.52	-0.18	Na_2SO_4
Thermonatrite	-6.17	-6.05	0.12	$Na_2CO_3:H_2O$
Tremolite	11.36	67.93	56.57	$Ca_2Mg_5Si_8O_{22}(OH)_2$

manganite (MnOOH), birnessite (MnO_2), manganese sulfide (MnS), and rhodochrosite ($MnCO_3$).

The precipitation of manganese oxides, and manganese hydroxides, is very obvious at a depth of about 0.1 m below the sediment surface. For the minerals manganite and birnessite, exemplifying a group of similar minerals, the saturation indices lie around zero. In deeper core regions these and all other oxides and hydroxides are in a state of undersaturation.

The slight but very constant supersaturation (saturation index about +0.5) found for the mineral rhodochrosite over the whole depth range between 0.2 and 12 m below the sediment surface is quite interesting as well. This can be understood as an indication for a new formation of the mineral in this particular range of depth. Below 13 m rhodochrosite and MnS are both *under*saturated, obviously absent in the solid phase, and therefore cannot have controlled the low manganese concentrations still prevalent in greater depths by means of mineral equilibria.

Calculation of Predominance Field Diagrams

The graphical representations of species distributions and/or mineral saturation as a function of E_H-value and pH-value, which are commonly typified as predominance field diagrams, or sometimes even not very correctly as stability field diagrams, can be done very accurately with the aid of geochemical model programs. The diagrams related to manganese, iron and copper shown in Chapter 11 (Figures 11.2, 11.4, and 11.16) as well as the Figure 15.2 referring to arsenic, have all been made by applying the model program PHREEQC.

The procedure consisted in scanning the whole E_H/pH range in narrow intervals with several thousand PHREEQC-calculations and a given specific configuration of concentrations (in this particular case an ocean water analysis at the ocean bottom, at the site of manganese nodule formation). Thus, each special case is individually calculated and adjusted in agreement to the appropriate temperature, the correct ionic strength (and hence the correct activity coefficient) and accounting for all essential aquatic species and all the minerals eventually present.

Such diagrams as these are not only much more closely adapted to the respective geochemical environment, but also contain essentially more information than the otherwise customary diagrams in which boundaries mostly result in a simplified

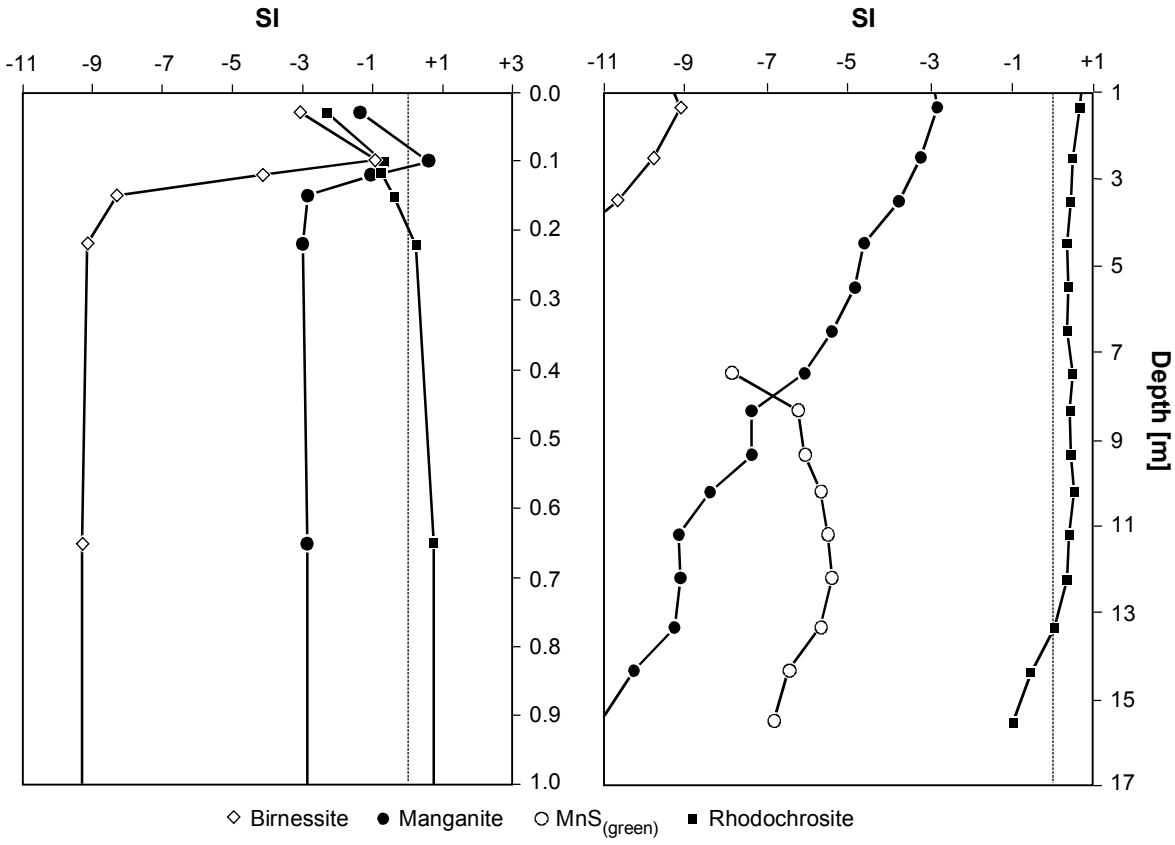

Fig. 15.1 Depth profiles of the saturation indices related to several manganese minerals in sediments approximately 4,000 m below the water surface, off the Congo Fan. The diagram depicted on the left-hand side covers the region close to the sediment surface; whereas the diagram on the right reflects the range down to the core's ultimate depth in another depth scale. Concentration profiles of the pore water pertaining to this core are shown in Figure 3.1; the concentration profile of manganese is shown in more detail in Figure 3.8, its diffusive fluxes are discussed more thoroughly in Section 3.2.3.

fashion from the given specific conditions. On the other hand, this information cannot any longer be included reasonably into one diagram only. Here, one diagram is used exclusively for the predominance field of aquatic species (left diagram), whereas a second is used to visualize the saturation ranges of the various minerals (right diagram). This makes sense inasmuch as, wherever minerals become supersaturated, there will nevertheless be an according distribution of the aquatic species that cannot simply be omitted in preference of the minerals. The diagrams shown on the right-hand side reflect the saturation ranges. Here, it is reasonable to depict overlapping ranges of various minerals, because which mineral might precipitate - and which one will not - is not determined on account of these statements or the degree of supersaturation.

Adjustment of Equilibria to Minerals and to the Gaseous Phase

Calcite is supersaturated in seawater which is described with regard to its solutes in the Tables 15.1 to 15.3. For calcite, the degree of supersaturation is expressed by the saturation index of 0.76, as shown in Table 15.3. Moreover, the partial pressures values of the gaseous phases pCO_2 and pO_2 (log pCO_2 = -3.38; log pO_2 = -0.70) are indicated which differ only slightly from the respective atmospheric values. Now it would make sense to ask what composition of this seawater is to be expected, if the equilibria were adjusted to the atmospheric CO_2 and O_2-partial pressure, and, for example, to the mineral calcite that eventually might need to be precipitated. Table 15.4 shows the result of such a calculation with regard to the essential properties of the solution. Naturally, the

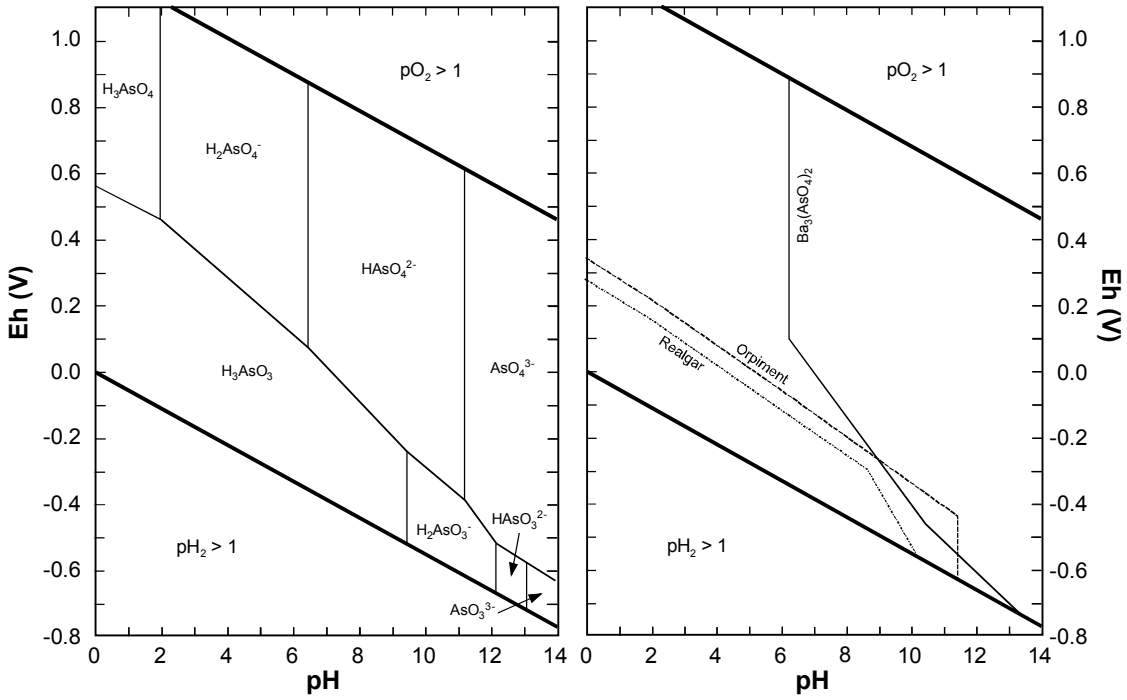

Fig. 15.2 Predominance Field Diagram for arsenic under the condition of manganese nodule formation at the bottom of the deep sea (after Glasby and Schulz 1999). The calculations in this diagram were performed with the model PHREEQC. The partial diagram on the left only represents the predominant ranges of the aquatic species. The diagram on the right covers the ranges of several minerals which are, under the given conditions, supersaturated (SI > 0).

program PHREEQC will then provide further detailed information on the distribution of the aquatic species and all the saturation indices according to the Tables 15.2 and 15.3, which presentation, however, was omitted in this context.

Decomposition of Organic Matter by Oxygen and Nitrate

If certain boundary conditions are maintained, the application of the model program PHREEQC leads to options of particular interest, whenever simulations of one, or several simultaneously running reactions are carried out. The oxidation of organic matter by dissolved oxygen - and after it is consumed, by nitrate - represents a very important reaction in seawater and especially in the sediment. In the model calculation presented in Figure 15.3 the following boundary conditions were selected: The seawater under study, or marine pore water, should be in a state of equilibrium with the mineral calcite at the beginning of the reaction and with a gaseous phase containing 21 % O_2 and 0.034 % CO_2. The composition of this water sample is summarized in Table 15.4. Organic substance containing amounts of nitrogen and phosphorus according to the

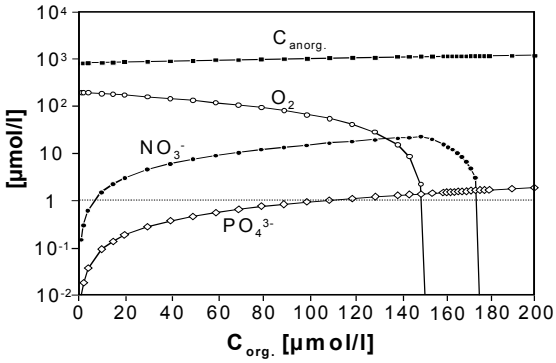

Fig. 15.3 Geochemical model calculation using the program PHREEQC. To an oxic seawater with calcite in equilibrium (cf. Table 15.4) an organic substance is gradually added automatically leading to a redox reaction. The system should continue to be open to calcite equilibrium, but sealed from the gaseous phase environment. First, free oxygen, and subsequently nitrate, will be consumed. Afterwards, the system shifts to the anoxic state (cf. continuance of reactions in Fig. 15.4).

Seawater from Nordstrom et al. (1979)

Phase	Si	log IAP	log KT
Calcite	0.00	-8.48	-8.47
CO_2 (g)	-3.47	-21.62	-18.15
O_2 (g)	-0.68	82.44	83.12
pH	=	7.902	Charge balance
pe	=	12.713	Adjusted to redox equilibrium
Ionic strength	=	6.734E-1	
Temperature (°C)	=	25.0	

Elements	*Molality*	
C	8.139E-4	Equilibrium with Calcite and pCO_2
Ca	9.876E-3	Equilibrium with Calcite
Cl	5.657E-1	not changed
Fe	3.711E-8	not changed
K	1.058E-2	not changed
Mg	5.507E-2	not changed
Mn	3.773E-9	not changed
N	6.571E-6	Adjusted to redox equilibrium
Na	4.854E-1	not changed
O(0)	3.951E-4	Equilibrium with pCO_2
S	2.93E-02	not changed
Si	7.382E-5	not changed

Table 15.4 In the seawater analyses shown in Tables 15.1 to 15.3, an equilibrium adaptation to the mineral calcite (SI = 0) and to the atmosphere with log pCO_2 = -3.47 (equivalent to pCO_2 = 0.00034) and log pO_2 = -0.68 (equivalent to pO_2 = 0.21) was calculated. This model calculation was performed with the program PHREEQC (Pankhurst 1995, Parkhurst and Appelo 1999).

Redfield ratio (Redfield 1958) of C:N:P = 106:16:1 (cf. Section 3.2.5) is then gradually added to this solution. Simplified, such a theoretical organic substance is composed of $(CH_2O)_{106}(NH_3)_{16}(H_3PO_4)_1$ or, divided by 106: $(CH_2O)_{1.0}(NH_3)_{0.15094}(H3PO4)_{0.009434}$. The horizontal axis in Figure 15.3 records the substance addition in terms of µmoles per liter. If the situation in the sediment is to be described, an equilibrium of calcite should exist as well. The system under study should not be open to the gaseous phase any more, instead, these influences should now be determined by the consumption of oxygen within the system and by the concomitant release of CO_2.

In the model, the organic substance added to the reaction automatically triggers a sequence of redox reactions which becomes evident due to the concentrations involved which are demonstrated in Figure 15.3. First, the concentration of oxygen declines, and the concentration of nitrate and phosphorus increases according to each of their proportions in the original organic substance. As soon as oxygen is consumed, nitrogen will be utilized for further oxidation of the continually added organic substance. Subsequently, the system shifts over to an anoxic state.

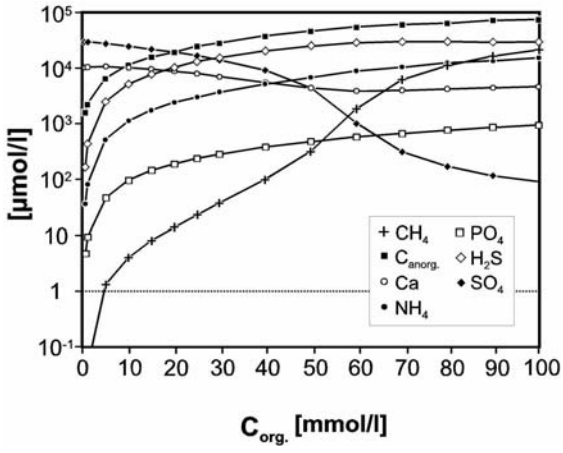

Fig. 15.4 Geochemical model calculation using the program PHREEQC. In an anoxic system (state at the end of the model calculation from Fig. 15.3), the gradual addition of organic matter to the redox reaction is continued, whereby the system is kept open for calcite equilibrium and sealed from the gaseous phase. Initially, the dissolved sulfate will be consumed, in the course of which low amounts (logarithmic scale) of methane will emerge. Only after the sulfate concentration has become sufficiently low, will the generation of methane display its distinct increase.

Decomposition of Organic Substance under Anoxic Conditions

An anoxic system, as obtained from the previous reaction sequence, will be capable of further ongoing reaction, if the supply of organic matter is continued and the reaction is held under the same boundary conditions. The result consists in the continuation of the processes shown in Figure 15.3. The outcome of this experiment is presented in Figure 15.4. Here as well, the horizontal axis is calibrated with regard to the added amounts of organic matter in terms of mmoles per liter.

As expected, the sulfate concentration in solution initially decreases at a swift rate and, concomitantly, low amounts of methane already emerge. Only after the concentration of sulfate falls under a certain level, will methane be released in substantial amounts. The permanently maintained calcite equilibrium will result, due to precipitation, in the depression of the concentration of dissolved calcium ions (compare Schulz et al. 1994).

The sequence of reactions, as described and modeled above, has naturally been well established and frequently documented ever since the publications made by Froelich et al. (1979). However, it should not be overlooked that these processes were not pre-determined for the modeling procedure, instead, they rather 'automatically' evolved from the fundamental geochemical data supporting the model as well as from the pre-set, although very generalized, starting and boundary conditions. During the entire model calculation procedure, all quantitatively important species, the complex aquatic species, as well as the activity coefficients related to these solutions, were invariably taken into account. The dissolution/precipitation of calcite, a realistic and also quite well known reaction, was employed for an adjustment of the mineral phase equilibrium. Such a system can be made more complex, almost at will, by specifically operating with additional mineral phases (e.g. iron minerals or manganese minerals) that dissolve eventually, provided they are present and the condition of undersaturation prevails, or are allowed to precipitate in the case of supersaturation. However, the simulation of such mineral equilibria requires a very profound knowledge of the specific reactions of mineral dissolution or precipitation in the system under study.

15.2 Analytical Solutions for Diffusion and Early Diagenetic Reactions

Analytical solutions for Fick's Second Law of Diffusion were already discussed in Chapter 3, Section 3.2.4, without taking diagenetic reaction into account. With a diffusion coefficient D_{sed}, which describes the diffusion inside the pore cavity of sediments, Fick's Second Law of Diffusion is stated as:

$$\frac{\partial C}{\partial t} = D_{sed} \cdot \frac{\partial^2 C}{\partial x^2} \qquad (15.5)$$

This partial differential equation has different solutions for particular configurations and boundary conditions. In Section 3.2.4 the following solution was presented:

$$C_{x,t} = C_0 + (C_{bw} - C_0) \cdot erfc\left(x \Big/ 2 \cdot \sqrt{(D_{sed} \cdot t)} \right) \qquad (15.6)$$

The solution of the equation yields the concentration $C_{x,t}$ at a specific point in time t and a specific

depth x below the sediment surface. Here, t=0 is a point in time at which the concentration C_0 prevails in the profile's entire pore water compartment. At all later points in time the bottom water displayed a constant value C_{bw}. An approximation for the complementary error function (erfc) according to Kinzelbach (1986) can be found in Section 3.2.4, where examples are given that employ this analytical solution of Fick's Second Law.

Advection and very simple reactions can also be included in Fick's Second Law of Diffusion (e.g. Boudreau 1997):

$$\frac{\partial C}{\partial t} = D_{sed} \cdot \frac{\partial^2 C}{\partial x^2} - v \cdot \frac{\partial C}{\partial x} - k \cdot C + R_{(x)} \qquad (15.7)$$

Here, *v* denotes the mean velocity of advection, and k is a rate constant of a reaction with first order kinetics. The last term in the equation $R_{(x)}$ is an unspecified source or sink related term which is determined by its dependence on the depth coordinate x. Instead of $R_{(x)}$, one might occasionally find the expression (ΣR_i) which emphasizes that actually the sum of different rates originating from various diagenetic processes should be considered (e.g. Berner 1980). Such reactions, still rather easy to cope with in mathematics, frequently consist of adsorption and desorption, as well as radioactive decay (first-order reaction kinetics). Sometimes even solubility and precipitation reactions, albeit the illicit simplification, are concealed among these processes of sorption, and sometimes even reactions of microbial decomposition are treated as first order kinetics.

These, or smaller variations of the equation, are occasionally referred to as 'general diagenetic equation', thus stating a rather simplistic comprehension of (bio)geochemistry in favor of a more mathematically minded approach. A comprehensive and elaborate treatment of the analytical solutions of the equation is presented by Boudreau (1997) who, in particular, considers its multiple variations and boundary conditions. Currently, this important book represents the 'state of the art' for the diagenesis researcher who is more interested in mathematics. For the more practical diagenesis scientist thinking in terms of (bio)geochemistry, this presentation remains somewhat unsatisfactory, despite the fact that it gives various inspirations and contributes to a vast number of important compilations (e.g. as to the state of knowledge on diffusion coefficients in the sediment). Ultimately, the (bio)geochemical applications of such a solution are in fact rather limited and illicitly restrict the complexity obtained by experimental measurement in the natural system.

In simpler stationary cases the author would always prefer solutions obtained by applying the 'Press-F9-method' (compare Section 15.3.1), simple explicit numerical two-step models (compare Section 15.3.2), and numerical solutions, particularly for non-stationary cases or in cases with complex reactions, by using models like STEADYSED1 or CoTReM (compare Section 15.3.3).

Van Cappellen and Gaillard (1996) gave indications that the activity coefficients in marine pore water, and the various complex species as well, need to be included as a very important part of the solution (also compare Sections 15.1.1 and 15.1.2). It has to be assumed that, for instance, the decomposition of sulfate via respective complex equilibria also affects the activity of other dissolved ions. Furthermore, it has to be considered that charged complexes and ions, transported by means of diffusion at different rates (differing diffusion coefficients !), must lead to a separation of the distributed charges in the course of transportation. The importance this has for the processes particularly taking place in the sediment is not yet sufficiently established. However, van Cappellen and Gaillard (1996) assume that such processes may probably be neglected in marine sediments as the charges there are essentially determined by sodium and chloride ions.

15.3 Numerical Solutions for Diagenetic Models

The previous section demonstrated that the analytical solutions of Fick's Second Law of Diffusion can only be applied to a very limited number of cases. Frequently, highly simplified boundary conditions have to be assumed which actually cannot be found in a natural environment. Additionally, the effort is almost always limited to merely one component dissolved in pore water, or to its behavior in space and/or time. Any complex relations between the numerous dissolved components, or even concentrations of complexes and ion pairs which become variable due to reaction sequences, or accordingly taking into account the difference between concentrations and activities, all are simply not regarded in the mathematical

solutions of diagenetic processes. Nevertheless, these multiple component processes do not constitute a rare exception but represent the normal case, and must be considered the more one becomes concerned with measuring natural systems.

The solution to this problem consists in the application of numerical solutions when diagenetic processes are modeled. Such numerical solutions always divide the continuum of reaction space and reaction time into discrete cells and discrete time intervals. If one divides up the continuum of space and time to a sufficient degree into discrete cells and time steps (which is not the decisive problem with the possibilities given by today's computers), one will be able to apply much simpler and better manageable conditions within the corresponding cells, and with regard to the expansion of a time interval, so that, in their entirety, they still will describe a complex system. Thus, it is possible, for example, to apply the two-step-procedure (Schulz and Reardon 1983), in which the individual observation of physical transport (advection, dispersion, diffusion) or any geochemical multiple component reaction is made feasible within one interval of time.

15.3.1 Simple Models with Spreadsheet Software ('Press-F9-Method')

Structure of a Worksheet and Oxygen/Nitrate Modeling

Normal spreadsheet software (e.g. Microsoft - Excel®) present tools especially suited for modeling stationary and not too complex systems. The well-understood decomposition of organic substance by dissolved oxygen, and the concomitant release of nitrate, will serve as an example. Nitrate is also utilized in the oxidation of organic substance in deeper sections of the diffusion controlled profile. Figure 15.5 demonstrates the result of such a model procedure, the details of which will be further discussed in the following.

Table 15.5 shows excerpts from the worksheet used for modeling the decomposition of organic substance mediated by oxygen and nitrate. In the upper frame of the worksheet there are - apart from the headline – single parameters and constants that will be used in the lower part of the worksheet; they will be discussed later in that particular context.

In the lower frames of Table 15.5 the actual worksheet is depicted in rows 11 to 61 that divide up the one-dimensional profile into 50 lines, which represent 50 discrete cells. The first column (A) contains the depth below the sediment surface. In the uppermost cell (11) this depth is set to zero and represents the bottom water zone immediately on top of the sediment. Line 61 is already beyond the boundary of the modeled area and will be discussed later in the context of setting the boundary conditions. In cell A12 to A61 the depth is increased by the value dx = 0.001 m per cell, as pre-selected in cell A6. The cell A12 contains the Excel® notation: =A11+$A$6. This field may be copied all the way down to field A61. In the next two columns (B) and (C) we find default porosity values (n) or diffusion coefficients (D_{sed}) valid for all cells. However, should the porosity constants or diffusion coefficients be known for the particular depth profile, then they may be entered individually into the respective cells. The columns (D), (E) and (F) are connected to each other by loops so that an error message will be announced,

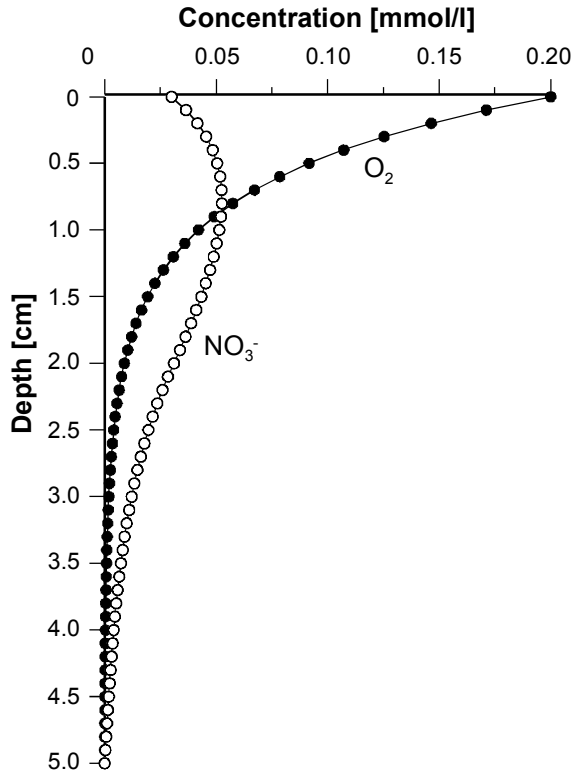

Fig. 15.5 Model of the decomposition of organic substance by dissolved oxygen and dissolved nitrate in a diffusion controlled pore water profile. Modeling was performed according to the 'Press-F9-method' with the spreadsheet software Excel®. Details pertaining to this model are explained in Table 15.5 and in the text.

Table 15.5 Worksheet (excerpts) from modeling the decomposition of organic substance by dissolved oxygen and dissolved nitrate in a diffusion controlled pore water profile. The model procedure was performed according to the 'Press-F9-method' with an Excel®. worksheet The columns are marked in the uppermost row with alphabetical characters, the rows are numbered in the first column. Details pertaining to the model are further explained in the text.

	A	B	C	D	E	F	G	H	I
1									
2	**Model oxidation C_{org} with oxygen and nitrate**						switch	C:N	$k(O_2)$
3							0	3.0	7.9E-09
4				----------	mmol l^{-1} = mol m^{-3}	----------			
5	dx(m)		dt(sec)	$C_0(O_2)$	$C_0(NO_3^-)$	$C_b(O_2)$	$C_b(NO_3^-)$		$k(NO_3^-)$
6	0.001		1.0E+06	0.2	0.03	0.0	0.0		3.2E-09
7									
8									
9	Depth	ϕ	Ds	O_2-Flux	O_2-Red.	O_2	NO_3^--Flux	NO_3^--Red.	NO_3^-
10	m		$m^2 sec^{-1}$	---------	mol m^{-2} s^{-1}	-----	mmol l^{-1}	---------	mol m^{-2} s^{-1} ----- mmol l^{-1}
11	0.000	0.60	5.4E-10	9.36E-09		2.00E-01	-2.11E-09		3.00E-02
12	0.001	0.60	5.4E-10	8.01E-09	1.35E-09	1.71E-01	-1.66E-09	0.00E+00	3.65E-02
13	0.002	0.60	5.4E-10	6.85E-09	1.16E-09	1.46E-01	-1.27E-09	0.00E+00	4.16E-02
14	0.003	0.60	5.4E-10	5.86E-09	9.90E-10	1.25E-01	-9.40E-10	0.00E+00	4.55E-02
					:				
					continued				
					:				
29	0.018	0.60	5.4E-10	5.65E-10	9.53E-11	1.21E-02	8.27E-10	0.00E+00	3.63E-02
30	0.019	0.60	5.4E-10	4.83E-10	8.16E-11	1.03E-02	8.55E-10	0.00E+00	3.37E-02
31	0.020	0.60	5.4E-10	4.13E-10	6.98E-11	8.83E-03	8.78E-10	0.00E+00	3.11E-02
32	0.021	0.60	5.4E-10	3.54E-10	5.97E-11	7.56E-03	8.07E-10	9.09E-11	2.84E-02
33	0.022	0.60	5.4E-10	3.03E-10	5.11E-11	6.46E-03	7.42E-10	8.29E-11	2.59E-02
34	0.023	0.60	5.4E-10	2.59E-10	4.37E-11	5.53E-03	6.81E-10	7.56E-11	2.36E-02
					:				
					continued				
					:				
55	0.044	0.60	5.4E-10	1.15E-11	1.40E-12	1.77E-04	1.30E-10	7.13E-12	2.23E-03
56	0.045	0.60	5.4E-10	1.04E-11	1.12E-12	1.41E-04	1.25E-10	5.84E-12	1.83E-03
57	0.046	0.60	5.4E-10	9.56E-12	8.62E-13	1.09E-04	1.20E-10	4.61E-12	1.44E-03
58	0.047	0.60	5.4E-10	8.93E-12	6.29E-13	7.96E-05	1.17E-10	3.42E-12	1.07E-03
59	0.048	0.60	5.4E-10	8.52E-12	4.11E-13	5.20E-05	1.15E-10	2.26E-12	7.07E-04
60	0.049	0.60	5.4E-10	8.32E-12	2.03E-13	2.57E-05	1.14E-10	1.13E-12	3.52E-04
61	0.050					0.00E+00			0.00E+00

if the appropriate Excel® setting ('Iterative Calculation') should not be selected. The diffusive O_2 flux is calculated by employing Fick's First Law of Diffusion (Equation 3.2 in Chapter 3), whereby the gradient obtained from the concentrations in column (F) is used. The concentrations in column (F) are calculated stepwise for each time interval from the preceding value, from the material flux in and out of the cell, and from the decomposition activity listed in column (D). Hence, the result in cell D11 reads in Excel® notation:

D11=B11*C11*((F11-F12)/$A$6)

D11 consequently contains the flux rate of material directed from the bottom water into the sediment. The cells D12 to D60 will be accordingly copied from this cell. Cell D61 remains empty.

The decomposition of organic substance in the uppermost sediment zone is written in the cell E12; cell E11 (bottom water) remains empty. In the example shown the decomposition of organic substance mediated by oxygen in a reaction following first order kinetics was still bound to the

yet prevalent oxygen concentration. This does not mean to say that this must always be so. As for the model, any other kinetic, or, in general terms, any other value could be assigned to the respective cells. As for the first order kinetics example, the line E12 reads in Excel® notation as follows:

E12=$I$3*F12

Cells E13 to E60 are copied from this cell accordingly, cell E61 remains empty. Column (F) contains O_2-concentrations, whereby cell F11 contains the upper boundary condition via a constant bottom water concentration. Cell F61 contains the concentration at the lower boundary - which in this particular case is equivalent to 0.0. The cell F12 is calculated from cell F12 (hence from its own previous value) as well as from the cells D11, D12, and E12, each multiplied with the length of the time interval. Written in Excel® notation this reads:

F12=IF($G$3;$D$6;F12+(D11*$C$6)-(D12*$C$6)-(E12*$C$6))

(The function 'IF' refers to the English version of Excel®, e.g. for the German version this function would be 'WENN'.)

Cells F13 to F60 are copied from this cell accordingly. Cell F61 contains the lower boundary conditions (in this case 0.0) which will be further dealt with later. It appears of practical importance at this point of calculation that there is the option of stopping the calculation procedure by means of a switch function. If the switch cell G3 assumes zero value the calculation will be performed. If the cell contains the value 1, then all concentrations will be adjusted to the value present in cell D6 (concentration in bottom water). Designing the structure of the worksheet, the switch should be set to a value of 1, in order to avoid unnecessary error messages due to references to not yet properly filled cells. Additionally, it is easy to rebuild the worksheet whenever ill-chosen conditions pertaining to the iteration have led to extreme values and/or oscillations.

Column (G) contains nitrate concentrations analogous to column (D) used for oxygen. In this example, the same diffusion coefficients were used to calculate the fluxes. Here, different individually adjusted coefficients can certainly also be used. Again, cell G11 contains the flux rate directed from the bottom water to the sediment and reads written in Excel® notation:

G11=B11*C11*((I11-I12)/$A$6)

Cells G12 to G60 are copied from this cell accordingly, whereas cell G61 remains empty. Column (H) contains the decomposition mediated by nitrate which can be set voluntarily, as has been the case in oxygen mediated decomposition. In this example, a decomposition of 0.0 has been pre-determined for the cells H12 to H31, as well as the assumption of first-order kinetics in cells H32 to H60. Here, too, it is not intended to claim that this allocation must necessarily be as shown in the example. As for the model, any other type of kinetics would be possible as well as any values set otherwise . Hence, cell H32 reads in Excel® notation:

H32=$I$6*I32

Cells H33 to H60 are copied from this cell accordingly. Cell H61 remains empty.

Analogous to column (F), column (I) this time contains the calculated nitrate concentrations which again are connected with loops to the columns (G) and (H). However, in the case of nitrate, there is also some release into the pore water fraction due to the oxygen mediated decomposition of organic substances. Thus, each cell belonging to column (I) is calculated from its previous value, from the diffusive import from above, from the diffusive export downwards, from the import from the oxidation of organic material mediated by oxygen (here, selective C:N ratio), as well as from the decomposition mediated by nitrate. For cell I12, this reads in Excel® notation as follows:

I12=IF($G$3;$E$6;I12+(G11*$C$6)-(G12*$C$6)+((1/$H$3)*E12*$C$6)-(H12*$C$6))

(The function 'IF' refers to the English version of Excel®, e.g. for the German version this function would be 'WENN'.)

Cells I13 to I60 are copied from this cell accordingly. Cell I11 contains the bottom water concentration as a fixed boundary condition, whereas cell I61 assumes the value of 0.0 as the concentration at the lower boundary. In this column it is also recommended to link the calculation performance to the operational 'switch' of cell G3.

The model is now finished and the essential margin values compiled in the upper frame of Table 15.5 are added. The switch in G3 is then set to zero. Now the key F9 (re-calculation of the worksheet) is repeatedly pressed until the figures in the worksheet do not (significantly) change, i.e., until a (practically) steady state is reached. Depending on the speed of the computer and the spreadsheet software used, this can take some few minutes, so that one can hold the F9-key down during that time.

At this point it needs to be clearly stated that only the final iterative steady state of the model provides a correct result, because the diffusive flux is calculated according to Fick's First Law of Diffusion in the columns (D) or (G) which is only valid when stationary conditions are provided. Even if time intervals of specific length are employed in the process of iteration, it is not permitted, by no means at all, to draw conclusions on the time necessary for reaching the steady state, since the columns (D) and (G), and consequently (F) and (I) as well, contain false information relative to each of the respective non-steady states.

The length of the time intervals (cell C6) is only a mechanism used for iteration, whereby too short intervals will result in an unnecessarily long pressing of the key F9, whereas too large intervals would lead to escalating oscillations within the model (in our example after about dt=2.3E6). Only after the steady state is reached will this 'false way' of the iteration become 'consigned to oblivion', and the result will be correct in all columns. Non-steady states and intervals prior to the development of particular concentration patterns can only be managed by applying Fick's Second Law of Diffusion, either in form of analytical solutions (cf. Section 15.2) or in form of numerical solutions (cf. Sections 15.3.2 and 15.3.3).

The concentration-dependent boundary conditions assigned to the model's upper-boundary limits (unspecified but constant concentrations in the cells F11 and I11) are relatively unproblematic since they represent a constant concentration in the bottom water zone. This is an imperative prerequisite for assuming a steady state in pore waters from superficial sediments. The condition for the lower boundary of the profile is somewhat more problematical. In the above example, the concentrations of both oxygen and nitrate were set to zero. In the model, this is tolerable as long as the value 0.0, constituting the lower boundary (within the limits) of the model, already results from the reactions, and as long as the set value 0.0 will not exert any practical influence on the lower parts of the profile. This 'zero concentration boundary condition' hence constitutes a 'zero flux boundary condition'. This also implies that the boundaries of the model must be extended downward until this state is sufficiently assumed. Selecting a zero concentration and, consequently a 'zero flux boundary condition', makes sense in this example, but it must not always be an adequate boundary condition. In the following example, we will consider the case in which a value is chosen which clearly deviates from 0.0 and thus indirectly provides a steady diffusive flux across the lower boundary.

Modeling the Reaction Sulfate/Methane

Niewöhner et al. (1998) describe profiles of pore water which were obtained from upwelling areas off the shores of Namibia. In these pore-water samples, sulfate reacted with methane in a ratio of 1:1. A similar example has already been introduced in Chapter 3 (Figure 3.31, also cf. Chapter 5), in context with problems occurring in methane analytics. In this example, the measured values will now be presented in Figure 15.6 together with the result of a model designed according to the 'Press-F9- method'.

In principle, the worksheet for the modeling of Figure 15.6 does not differ very much from the one described previously, so that it does not demand special description. The essential features of this model are:

The decomposition of methane and sulfate (cf. Chapter 8) occur for both reactants in specific depths at identical rates which were entered into the spreadsheet. The adjustment to the measured profiles was committed only by these (microbial) decomposition rates. The decomposition parameter is set to 0.0 in all other cells, so that a diffusion controlled transport occurs with a constant concentration gradient.

The concentration of the upper boundary condition for the model is again provided by the appropriate bottom water concentrations: sulfate = 28 mmoles/l; methane = 0.0 mmoles/l.

The concentration of the lower boundary condition for sulfate is 0.0 mmol/l, since it was decomposed to 0.0 mmol/l long before the lower boundary of the model had been reached. However, the concentration of the lower boundary

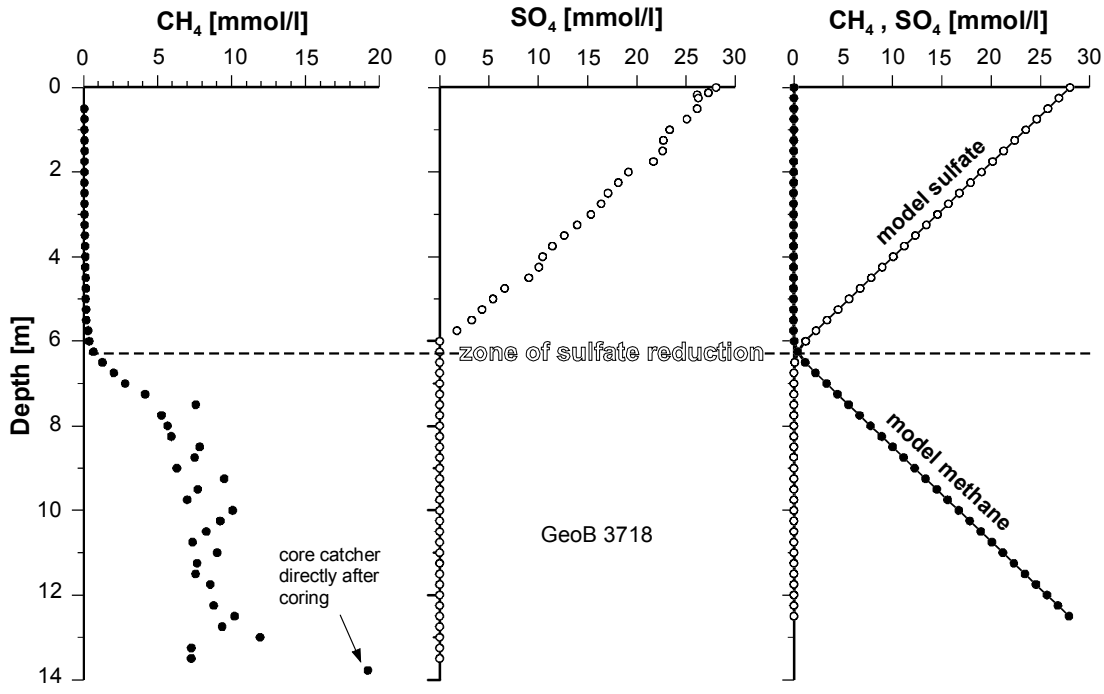

Fig. 15.6 Model results of the mutual decomposition of sulfate and methane as a 1:1-reaction in a diffusion controlled pore water profile. Modeling was performed according to the 'Press-F9-method' using the standard software Excel®. Details pertaining to the model and the calibration with data from a measured pore-water profile obtained from an upwelling area off Namibia (Niewöhner et al. 1998) are discussed in the text.

condition for methane has been concluded on the basis of pre-determining a steady decomposition in the same amount as for sulfate, and that this decomposition should continue in a specific depth until the value 0.0 is reached.

15.3.2 Two-Step Models with Explicit Numerical Solution of Fick's 2nd Law

In order to adequately account for the time course of processes which are mainly governed by diffusion, Fick's Second Law of Diffusion must be applied without exception (Equation 15.5). After all, Fick's First Law does not account for time at all. The analytical solutions described in Sections 3.2.4 and 15.2 and referring to Fick's Second Law may permit the calculation of a distribution of concentrations at a certain point in time, however, they apply to inert, non-reacting compounds. Only very specific and very simple reaction types, such as the completely reversible adsorption/desorption of a compound or its degradation following first-order kinetics can be included in analytical solutions. All reactions of higher complexity - and these encompass actually all the processes of early diagenesis - require reactions which are distinguished by the interdependencies between the various reactants and thus evade an analytical solution in which a distribution of concentrations has to be calculated in a single step, starting out from a given initial concentration.

Adequately modeling the combination of the physical transport by means of diffusion (including advection) on the one hand, and reactions which may be as complex as you like on the other, demands a subdivision of both the continuum of time and the transport pathway into discrete time intervals and discrete sections or cells, respectively. In each time step the physical transport of each cell belonging to the transport pathway under study is then calculated relative to each of the other cells, just as if the compound would not undergo reactions. Then the transport process is quasi brought to a halt and the concentrations in all cells will be changed just as if any imaginable (bio) geochemical reaction had in fact taken place. There is actually no type of reac-

tion that cannot be applied for mathematical reasons in this regard. Then physical transport is calculated once again on the basis of the concentrations thus calculated, followed by a subsequent calculation of the reactions etc. This procedure is referred to as the "Two-Step Method" or "Operator Splitting". It will be discussed more thoroughly in the following. As much as we know, this method has been applied for the first time by Schulz and Readon (1983). Here, only the simplest form of such a modeling process, the so-called explicit solution, will be presented for introductory purposes. It rapidly illustrates the principle of the Two-Step Method and suffices completely to achieve adequate modeling results in most practical situations.

The explicit solution (e.g. Kinzelbach 1986; Sieger 1993; Landenberger 1998) calculates a concentration $C_{x,t+t}$ as the concentration at location x of the transport pathway with respect to the future time point (t+Δt), whereby Δt denotes the length of the time step:

$$C_{x,t+\Delta t} = C_{x,t} + \Delta t \left[\begin{array}{l} D_{sed} \left(\dfrac{C_{x+\Delta x,t} - 2 \cdot C_{x,t} + C_{x-\Delta x,t}}{\Delta x^2} \right) \\ -v_a \left(\dfrac{C_{x+\Delta x,t} - C_{x-\Delta x,t}}{2 \cdot \Delta x} \right) \end{array} \right] \qquad (15.8)$$

Only concentrations at the known time point t are used on the right side of the equation sign for the same location x on the transport pathway, next to the two neighboring cells (x+ Δx) and (x-Δx), whereby Δx denotes the cellular length of the transport pathway. D_{sed} is the diffusion coefficient of the compound under study (Section 3.2.2). To a certain extent, the equation also permits the inclusion of advection with the flow velocity v_a. If v_a = 0.0, then only diffusion will be effective. However, in cases of greater flow velocities the much greater dispersion coefficient must be applied instead of the diffusion coefficient D_{sed}. Its dimension depends on the flow velocity. Such fluxes, including the adjusted dispersion coefficients, are preferably significant for the flow properties of groundwater in sandy aquifer (Schulz 2004).

Equation 15.8 hence permits the calculation of the distribution of concentrations in all cells of a transport pathway at the end of a given time period, starting out from any distribution of concentrations prevailing at the beginning. Somewhat problematical is merely the first (uppermost) cell and the last (lowest) cell of the given pathway, for each of these cells lack a neighboring cell either above or below it, a condition which Equation 15.8 demands to be fulfilled by all cells. This normally does not lead to a problem for the first, uppermost cell. It represents the bottom water above the sediment package and thus contains a constant or, at least, a time-specific concentration. The last, or lowest, cell presents more difficulty, as various margin conditions can be selected. Here, an example could consist in a constant or, at least, time-specific concentration as well. Another possibility would be an extension of the concentration gradient from the third-last cell over the second-last to the ultimately last cell. At least Equation 15.8 is only applied to the cells 2 to (n-1) in a series of n cells, and not to the cells 1 and n.

Each of the two variants applicable to determine the concentration in the last, lowest cell of the transport pathway have a flaw. A constant value for the concentration in this cell demands that, during model calculation, a concentration deviating essentially from this value by way of diffusion or reaction should never approach the lower margin, where the model calculation would be influenced by a constant value, without being capable of influencing this value itself. For example, if the constant value were 0.0, all higher concentrations appearing in the proximity would quasi become "swallowed". For this reason, the model territory always has to be defined large enough to ensure that this will never be the case. Such an effect does not appear with the same intensity in the second variant, which is used to determine the concentration at the lower margin by means of a constant gradient, but this solution also produces problems. The small errors which arise from the extrapolation of the gradient can add up to quite remarkable deviations in the course of numerous time steps. It is best to define the model territory large enough to avoid that the gradient near the lower margin will not essentially differ from 0.0 at any given concentration.

The explicit solution permits simple straightforward modeling, but has the disadvantage that the length of a time-step is very closely bound to the length of a cell and to the diffusion coefficient. Very unpleasant oscillations frequently appear which rapidly add up to values lying outside the permissible numerical range if the time-steps become too large. Equation 15.9 describes a maximum length a time-step may assume,

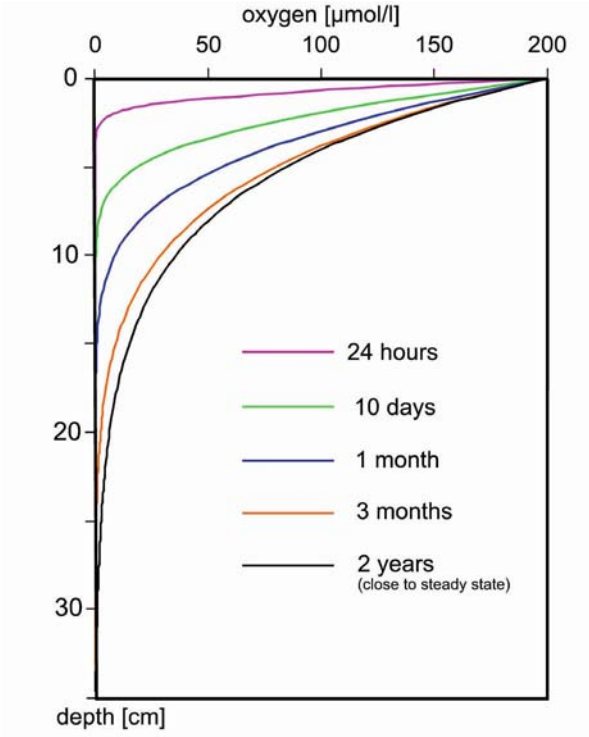

Fig. 15.7 Calculation of the equilibrium between oxygen consumption occurring during the oxidation of sedimentary organic matter near the sediment surface and resupply of oxygen by means of diffusion. Here, oxygen consumption is assumed to follow first-order kinetics. Application of Fick's Second Law in an explicit numeric solution permits a reliable calculation of the times required for the adjustment of a stationary condition.

whereby distinctly shorter time-steps may also be used without causing any problem.

$$\Delta t \leq \frac{\Delta x^2}{2 \cdot D_{sed}} \qquad 15.9$$

The explicit solution can be realized quite reasonably with an Excel® worksheet in the sense of the ‚Press-F9-Method' (Section 15.3.1). However, in most cases a program written in a higher programming language will be applied, since this type of modeling is made *because* one desires to include more complex (bio)geochemical reactions. And sooner or later the limits of modeling are reached when an Excel® worksheet is used.

An easy to handle and rather generally designed computer model written in FORTRAN (EXPLICIT.FOR) can be downloaded on the internet at:

http://www.geochemie.uni-bremen.de/downloads/

along with brief user instructions written in English and data sets pertaining to several examples.

The following examples (Example 1 and 2) were calculated using this program. Subsequent examples (Examples 3 and 4) reveal how an explicit solution was realized with an Excel® worksheet in the sense of the ‚Press-F9-Method' (Section 15.3.1). Downloads of these worksheets are also available at the above mentioned internet address.

Example 1: Non-steady state development of an oxygen profile

An oxygen concentration profile such as the one which has been measured in situ (Fig. 3.5) or modeled (Fig. 15.5) is mostly interpreted in terms of a stationary condition (steady state) resulting from the consumption of oxygen in the sediment and its resupply by means of diffusion. Its consumption in the sediment is due to the oxidation of organic matter and other redox processes, such as the re-oxidation of divalent manganese. But how long does it take until such a stationary condition is reached ?

Figure 15.7 shows an example for the development of a steady-state condition starting out from an extreme initial situation. The explicit solution to Equation 15.8 always requires an initial situation, a concentration profile from which the following profiles of the subsequent time-step are calculated. In this example, an oxygen concentration of 0.0 was chosen as the initial situation underlying the entire profile. In principle, it does not make any difference what kind of initial concentration profile is used to reach the steady-state concentration profile. The initial profile will be "lost", at the latest, after a steady state is reached. Only the time necessary to reach the steady state will differ. The more the initial situation already resembles the steady state, the shorter the time until this condition will be reached - and vice-versa.

In this example, the oxygen consumption in each cell was calculated by applying first-order kinetics, which means that, in this case, oxygen is depleted with a half-life of 50 days. This is only but one possibility imaginable, other rates or kinetics of degradation are also possible and can be applied in the model accordingly. The half-life of 50 days represents a sediment distinguished by a relatively poor turnover. Naturally, there is no consumption at the beginning when no oxygen is

present in the entire profile. But any oxygen supplied from the bottom water into the sediment by means of diffusion will be immediately subject to the already mentioned consumption of oxygen displaying a half-life of 50 days.

If the sedimentary diffusion coefficient is given, the position of stationary condition will then be merely a function of the degradation rate, hence the half-life assumed in our example. Figure 15.7 illustrates that a concentration profile close to the stationary condition is reached within a time period as short as three months. This is the case even in our example in which the penetration depth of oxygen is at about 30 cm, and despite the fact that the initial concentration of 0.0 over the entire profile is far away from the stationary condition.

Example 2: Dating a sediment slide at the continental slope

While the previous example presents a purely theoretical case, Example 2 refers to a real situation (Zabel and Schulz 2001). The data shown in Figure 15.8 represent material from the cores sampled with a gravity corer at a water depth of approximately 4,000 m on the deep-sea fan off the estuary of the Congo River (Locations GeoB1401 and GeoB4914). Further pore-water profiles from Location GeoB1401 are also shown in Fig. 3.1.

Particularly the sulfate profile in pore water (center diagram in Fig. 15.8) was difficult to interpret as a picture showing a steady-state condition, for one would expect a nearly constant gradient that reaches down to the sulfate-methane transition zone (e.g. Niewöhner et al. 1998). Figure 3.6 shows such a measured profile. The sulfate profile depicted in Figure 15.8., however, displays a distinct alteration in the gradient at a depth range between 8 m and approximately 10 m. This would normally be explained with a re-oxidation of sulfide yielding sulfate under stationary conditions. However, oxygen and nitrate are not available for the reaction, as they have already been exhausted in the uppermost centimeters of this very reactive sediment. A re-oxidation reaction of sulfide with trivalent iron originating from the solid phase of the sediment would be imaginable theoretically, but this possibility was ruled out because the trivalent iron content of the sediment and the low sedimentation rate (approximately 5 cm kyr^{-1} , as derived from the left diagram in Fig. 15.8) account for a flux of trivalent iron to the reaction site which would be markedly too low - by more than a power of magnitude.

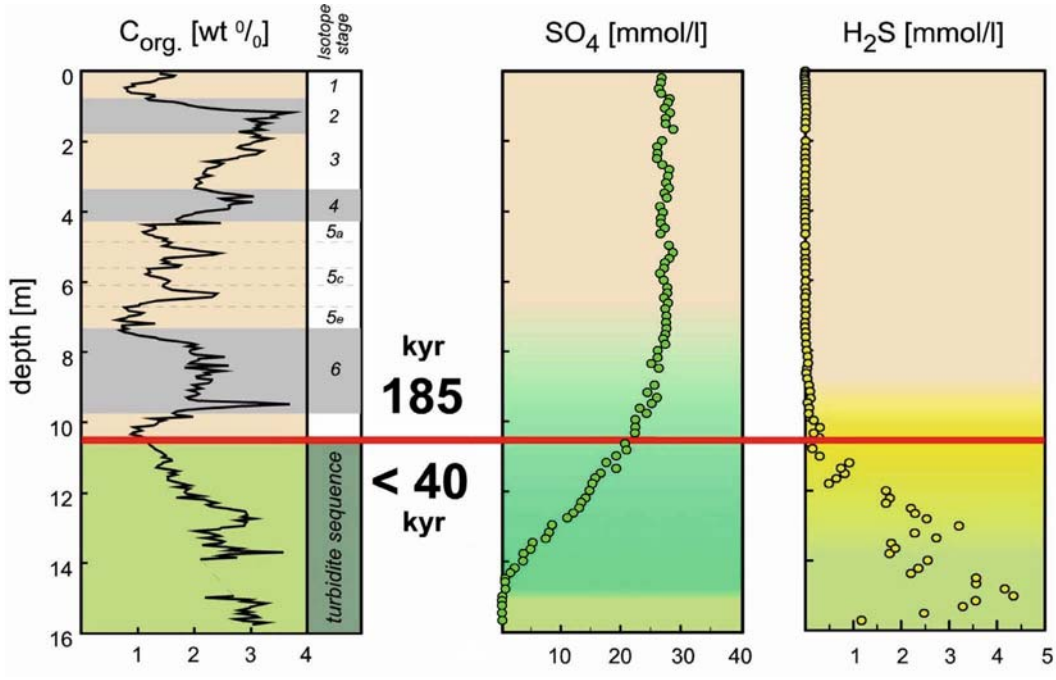

Fig. 15.8 Geochemical data obtained from a sediment core originating from a depth a 4,000 m off the Congo-River estuary (GeoB1401, GeoB4914) (Zabel and Schulz 2001). Left: C_{org} concentration and isotope stages. Center: Sulfate concentrations in pore water. Right: Sulfide concentrations in pore water. The red line crossing all profiles denotes a leap in time which is understood as an old surface, a basis of a sediment slide.

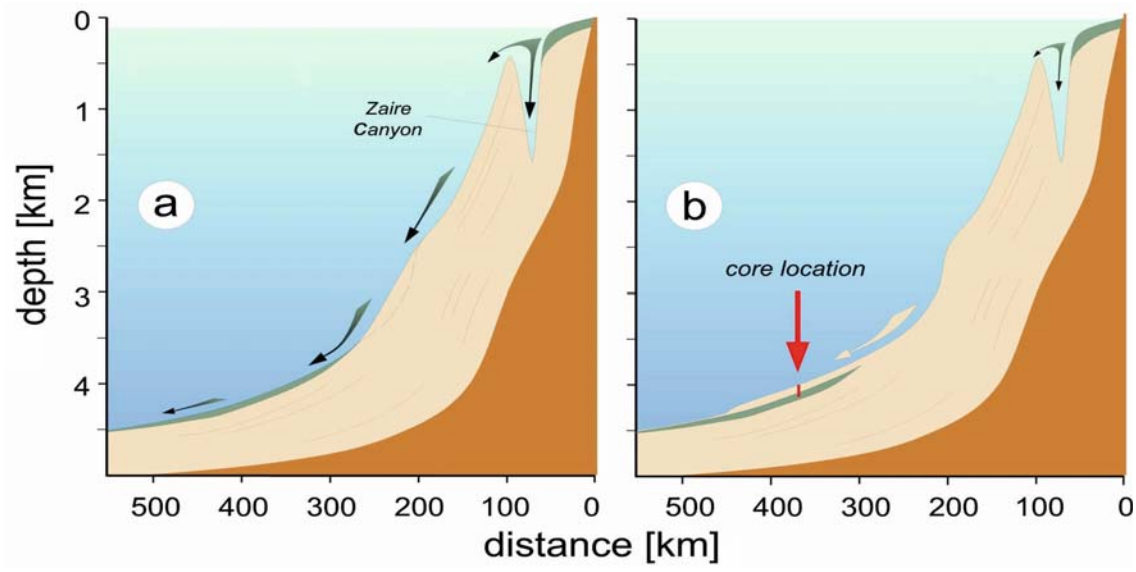

Fig. 15.9 Model concepts related to the development of the situation shown in Fig. 15.8. The left diagram displays the development of turbidite currents rich in organic matter at a water depth of approx. 4,000 m. The right diagram shows how the slide of an internally unperturbed sediment package covers these turbidite layers (Zabel and Schulz 2001).

A solution to this problem is only gained when this profile is interpreted as a non-state condition (Zabel and Schulz 2001), assuming that in recent geological time an approximately 10 m-thick sediment block slid over a very young series of turbidites which were rich in organic matter. This sediment slide must have proceeded so slowly that the sediment block remained unperturbed in its interior stratigraphy. Figure 15.9 shows the model concept which provided the basis in subsequent modeling of the pore water concentration profiles. The left diagram shows the situation before the slide when turbidite currents, rich in organic matter and originating from the overflow of the Zaire Canyon onto the deep-sea fan, had reached a depth of 4,000 meters. The right diagram shows the situation after the slide, including the sampling site of the sediment core examined.

But when did this slide occur? As a steady-state condition has quite obviously not been reached yet, a time-correct model according to Fick's Law and the Two-Step Method must be used to answer the question.

Figure 15.10 demonstrates in its left side the initial situation, hence the situation immediately after the slide in terms of sulfate and methane concentration profiles and alkalinity. Underneath the slide, i.e at the former sediment surface, a steady-state condition with a constant gradient reaching down to the sulfate-methane transition zone was then anticipated. We are familiar with such profiles from highly reactive sediments, for example, those obtained from the Congo Deep-Sea Fan. Unperturbed gradients displaying markedly less biogeochemical turnovers were applied to the sediment package lying on top of the sedimentary slide mass as the initial situation. We also know about such profiles in sediment cores originating from locations somewhat higher on this continental slope.

The right diagram in Figure 15.10 shows the modeling of a non-steady state condition about 300 years after the slide. The mutual degradation of sulfate and methane at the sulfate-methane transition zone and the release of bicarbonate (represented by alkalinity) were stoichiometrically applied as the involved geochemical processes according to the extent of methane oxidation. The model calculation was terminated after achieving a good visual adjustment of the calculated sulfate profile to the measured data. It clearly shows that this modeling procedure is able to explain entirely the measured concentration profiles of sulfate, methane, alkalinity and ammonia (not shown). Since the model was run using the correct time and the correct diffusion coefficients, anticipating that the slide incidence had taken place at about 300 years before the measurement of the concentration profiles may also be assumed to be correct. The potential error of the visual adjustment of the

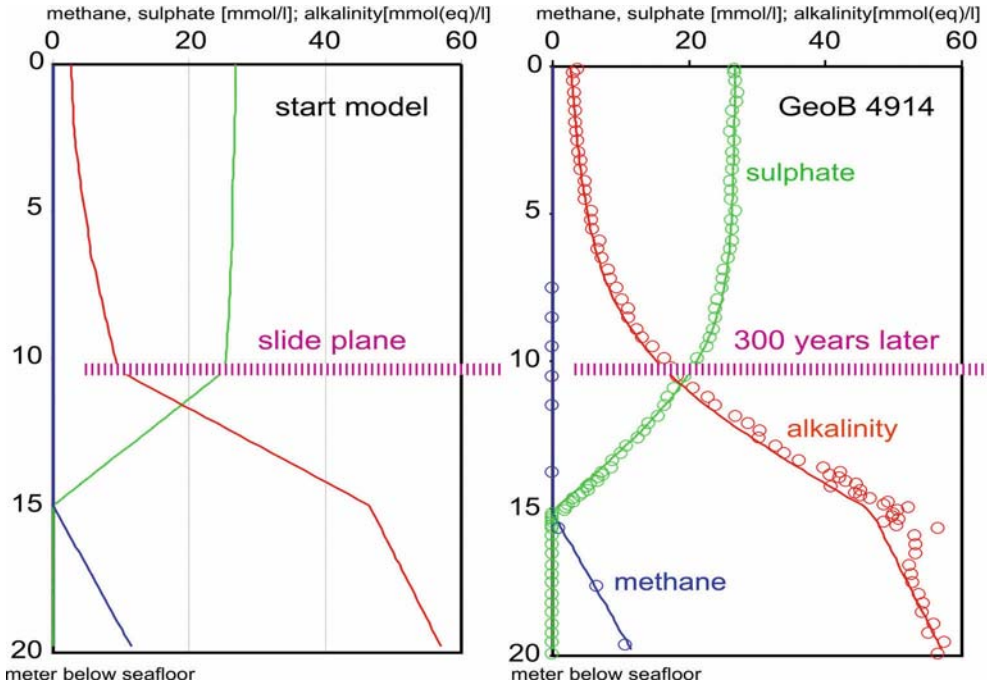

Fig. 15.10 Model calculation of sulfate in pore water, alkalinity and methane in an explicit numeric solution of Fick's Second Law, accounting for the reaction between sulfate and methane and the alkalinty which is affected thereby. The adjustment to the measured profiles depends on the time passed since the slide occurrence and thus permits the reconstruction of the time of its occurrence which took place about 300 years ago.

sulfate profile for the time span modeled is estimated to be somewhere between 5 to 10 % of this value.

Example 3: Reconstruction of the date of a sediment avalanche at the continental slope

Example 3 also illustrates the modeling of a sulfate profile really measured, including a sulfate-methane transition zone in the deep part of the profile. However, in this case the profile displayed such an unusual course that its interpretation as a steady-state condition did not appear justified by any means. As a consequence, this profile rested among many other measurement data for almost ten years. Only after we understood that non-steady-state conditions in marine sediment profiles - particularly in the continental slope region - are much more frequent than previously assumed were we able to understand this profile as well (Hensen et al. 2003).

The rather steep continental slope off the coast of Uruguay is distinguished by frequent irregular sedimentary transport events. Not only turbidity currents but also slides of relatively unperturbed sediment packages occur here, such as sediment avalanches. In case of sediment avalanches the originally stratified sediment layer is mostly destroyed and dissolved into single blocks. However, the original sediment is not dissolved all the way down to each single grain as is the case with turbidite currents. Figure 15.11 shows a section of the same profile above the continental slope, where the examined core was sampled with a gravity corer (GeoB2809, Bleil et al. 1994). The sediment avalanche which had been deposited at this location can be clearly recognized in the lower part of this sediment acoustic profile as it lies, practically without displaying any structure, on top of the otherwise layered sediments. Once again, the non-steady state progression of the sulfate profile in the pore water would provide us with information on the age of the avalanche.

Figure 15.12 shows the result of a non-steady-state model run which was performed by applying the explicit solution according to the Two-Step Method, this time with an Excel® worksheet according to the ‚Press-F9-Method'. This worksheet can also be downloaded from the above-

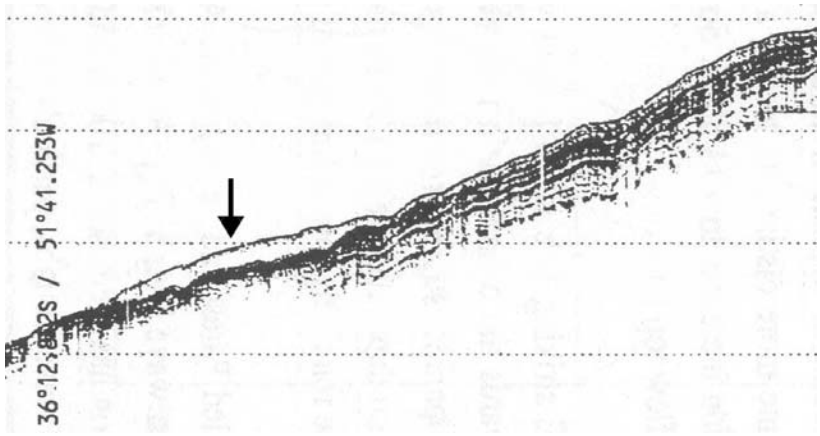

Fig. 15.11 Sediment-acoustic profile (PARASOUND) of the continental slope off the coast of Uruguay (Bleil and participants 1994). A sediment avalanche is recognizable below deposited as a compact sediment. The sediment core GeoB2809 also originated from this profile, including the pore water profiles shown in Fig. 15.12. (see also Hensen et al. 2003).

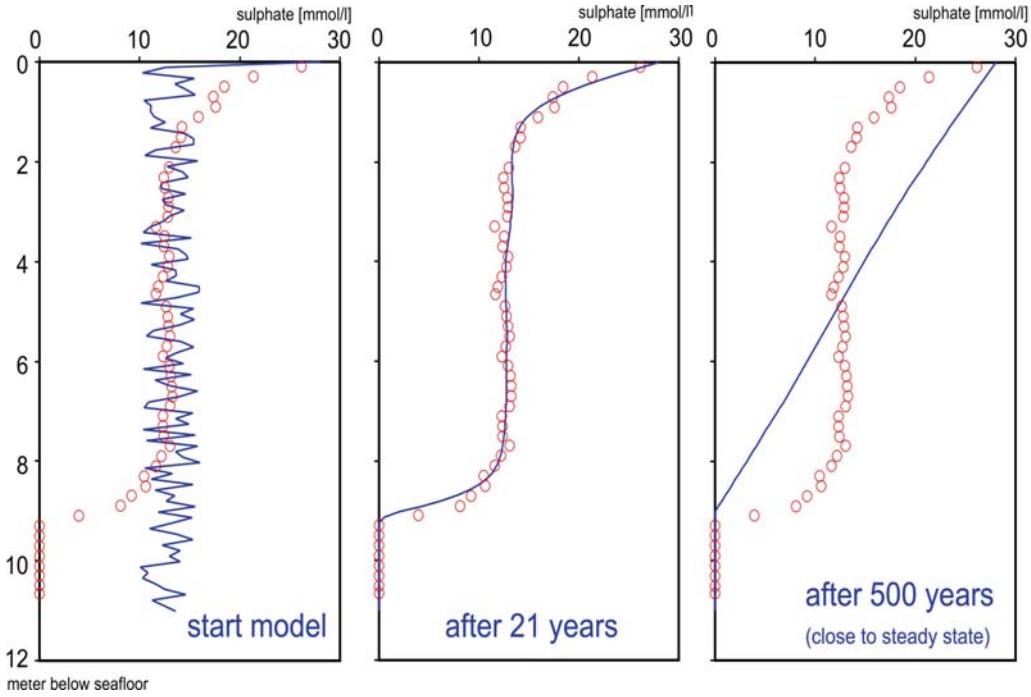

Fig. 15.12 Model calculation of the sulfate concentration profile in the deposition of a sediment avalanche on the continental slope off the coast of Uruguay (see also. Fig. 15.11). Red circles denote the measured sulfate concentrations. Blue lines indicate the model calculation at various time points after the avalanche: Left: Immediately after the occurrence of the avalanche. Center: approx. 21 years later. Right: approx. 500 years later.

mentioned website. The measured sulfate concentrations are marked by red circles in all partial diagrams of Figure 15.12. The left diagram shows in blue color the initial situation once again immediately after the deposition of the sediment avalanche. In this case, it was assumed that the concentration profile before the incidence of the avalanche decreased linearly from the concentration in ocean water (28 mmol l^{-1}) at the sediment surface down to a concentration of 0.0 in the region at the sulfate-methane transition zone. The profile was then perturbed by the avalanche, yielding irregular concentrations over the entire profile which scattered around the average of the ocean water values and the 0.0 value. This distribution of initial concentrations was calculated as a somewhat randomized 50 % ocean water concentration.

Starting out from this profile of initial concentrations, we then only introduced the time-correct diffusion in the model calculation, along with a correct diffusion coefficient, and the mutual degradation of sulfate and methane at the sulfate-methane transition zone.

First, the minor, randomly occurring differences between adjoining points were 'smoothed out' in the course of model calculation. At the same time, the upper part of the profile adapted more and more to the ocean water transition, while the lower part adapted to the low concentration of the sulfate-methane transition zone. After somewhat more than 20 years, an almost perfect adjustment to the measured profile was achieved without any other fitting technique (center diagram in Fig. 15.12). This core was obtained in 1994, and the sulfate profile was measured in the same year. The sediment avalanche consequently took place in the early 70s of the last century. The right diagram in Figure 15.12 shows the same profile model as it would look like in 500 years after the event. A new, almost stationary condition will be reached after this time, and only a faint suggestion of the S-shaped curve typical of the non-steady state condition will still remain recognizable.

Example 4: Formation of phosphorite in shelf sediments

It has been recently demonstrated in shelf sediments of the highly productive upwelling area off the coast of Namibia that certain sulfur bacteria release very high concentrations of phosphate into the pore water near the sediment surface. This produces a stratified precipitation of phosphorite minerals (Schulz and Schulz 2005). The questions to be answered by modeling are as follows:

- At which phosphate concentration must we expect the precipitation of which minerals ?
- The concentrations in pore water at a depth of only one centimeter below the sediment surface are considered as stationary. What release rates applying to phosphate must we postulate for the bacteria if it is known from experiments that the precipitation kinetics of phosphate minerals are in a certain range, and if the measured concentration profile in pore water is to be simulated correctly?
- How much time does it take for sulfur bacteria to release these phosphate concentrations till the amounts of phosphate found in the solid phase of the sediment accumulated ?

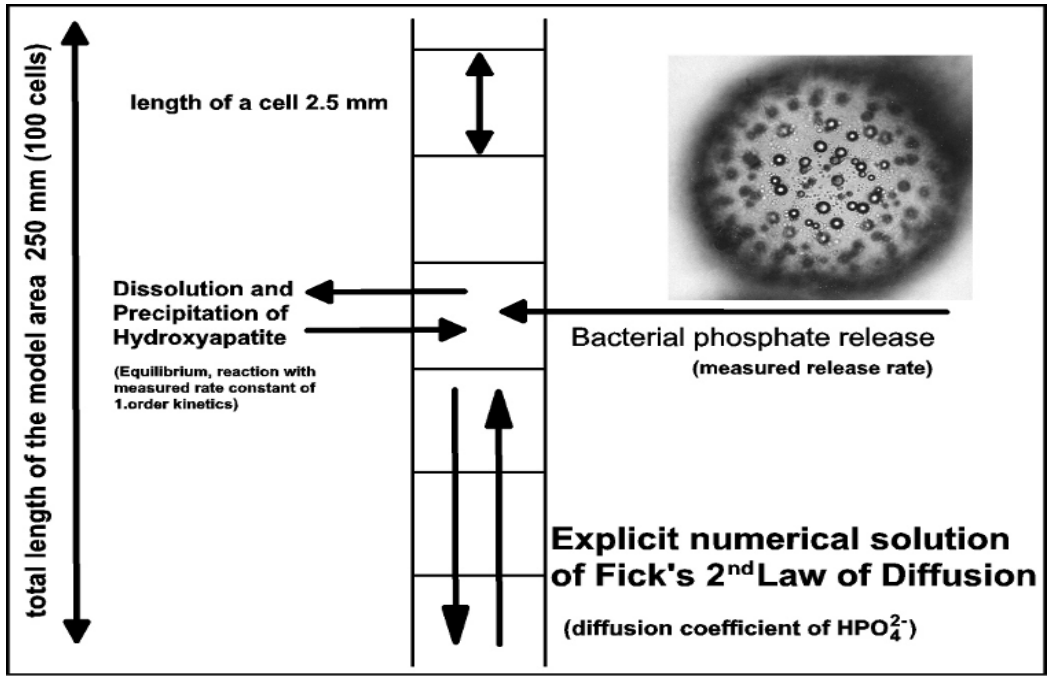

Fig. 15.13 Model concept about the development of phosphorite layer in an anoxic sediment on the shelf off the coast of Namibia (Schulz and Schulz 2005). Phosphate released by bacteria (*Thiomargarita*) reaches a stationary condition in pore water which is determined by release rates, precipitation and diffusion-dependent transport.

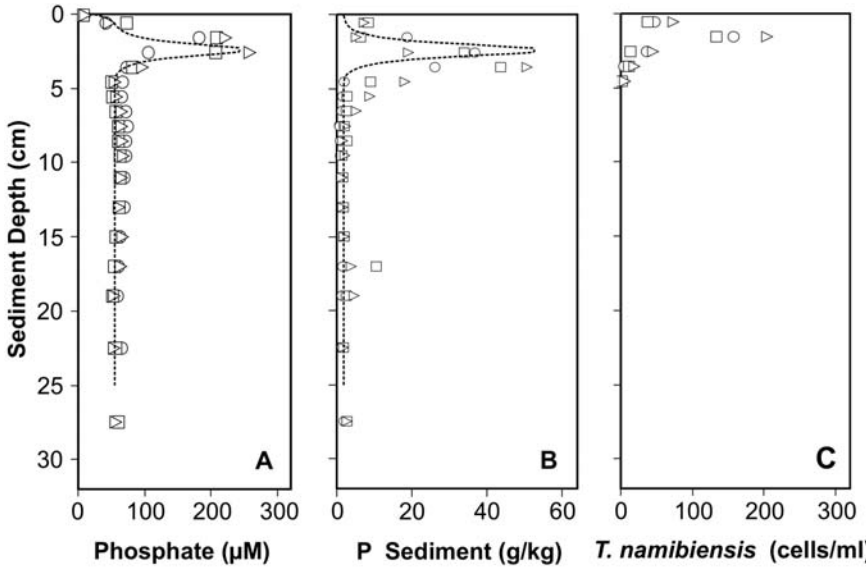

Fig. 15.14 Measured values and model calculation related to the model concept shown in Fig. 15.13. Open circles, triangles and squares denote the measured values of three parallel cores. The broken line curves represent the model calculation. Left: phosphate concentrations in pore water. Center: Sedimentary contents of phosphorus. Right: Bacterial cell counts in the sediment (after Schulz and Schulz 2005).

- How fast or slow is the phosphate mineral layer embedded in the sediment re-dissolved if phosphate concentrations increasing in the process of dissolution return to the ocean water by diffusion ?

Figure 15.13 shows the principle structure of the model which is supposed to give an answer to these questions. Here, realization was done in accordance with the explicit solution and the Two-Step Method using an Excel® worksheet, which can also be downloaded from the above mentioned website, along with other relevant information.

The model will record the upper 25 centimeters of the sediment if there are 100 cells each measuring a length of merely 2.5 mm. This accounts for a sufficiently good depth resolution in the interesting range of reactions, and it reaches deep enough so that the sensitive lower margin of the model is by no means influenced by the processes running inside the model. Apart from the time-correct diffusion of dissolved phosphate, a rate-controlled input (bacterial release of phosphate into the pore water fraction) and a rate-controlled output (precipitation of a phosphate mineral) are accounted for. Simultaneously all precipitations and dissolutions had to be recorded so that the total of precipitated phosphate could be compared with the sedimentary contents found in nature.

The input was only given for cells in which the presence of these large sulfur bacteria of the genus *Thiomargarita* that are even easily visible with the naked eye has been known to exist at the respective sediment depths. Precipitation of the mineral hydroxyapatite [$Ca_5OH(PO_4)_3$] was conducted with first-order kinetics as soon as the saturation concentration (40 µmol l^{-1} phosphate) was exceeded. This concentration resulted from model calculations performed with the program PHREEQC (Section 15.1.2) on this mineral which is characteristic for such conditions and whose presence in this sediment appeared to be likely on account of x-ray diffractometry (XRD).

The results of measurements made with natural sediments are compiled in Figure 15.14, together with the results of the model calculations. Both pore water concentrations and the contents in the solid phase of the sediment were absolutely correctly simulated considering the range of available measurement accuracy and reproducibility.

The above questions concerning modeling can thus be answered, and the answers concomitantly describe the circumstances of the development of marine phosphorite deposits by sulfur bacteria:

- The specific situation of pore water concentrations at this location yielded a phosphate

concentration of 40 µmol l^{-1} which is required in order to obtain saturation in the pore water fraction relative to the mineral hydroxyapatite which is known as a primary precipitate of phosphorite deposits.

- Phosphate release rates of sulfur bacteria ranging from 0.024 to 0.08 pmol l^{-1} $cell^{-1}$ had to be postulated. In case of higher release rates, calcium which is required for the precipitation of hydroxyapatite [$Ca_5OH(PO_4)_3$] could not have been supplied fast enough by means of diffusion. In case of a lower release rate, diffusion would have caused a distinctly broader spreading of the concentration peak in the pore water fraction than the peak measured. A phosphate release rate of 0.011 to 0.028 pmol l^{-1} $cell^{-1}$ for the bacteria was found in laboratory experiments. This range is very close to the postulated values, both ranges even overlap to certain extent. That the bacteria did not produce the highest release rates of the model may be explained with the fact that they simply did not appreciate their state of 'captivity' as much as their life in the wild. A precipitation rate applicable to hydroxyapatite emerged almost incidentally, which was also verified in laboratory experiments.
- Anticipating the fastest release rate of 0.08 pmol l^{-1} $cell^{-1}$ it will take only three months until the contents measured in the sediment are reached. In case of the lowest rate of 0.024 pmol l^{-1} $cell^{-1}$ it will take 14 months. Both values are plausible also against the background of sedimentation rates on the shelf.
- The phosphorite layers are quite well protected after being embedded in the sediment, for concentrations produced by the dissolution of these layers need a very long time to return to the sediment surface by diffusion. Even after 100 modeled years, the phosphate contents in the sediment will be only slightly lower than they were at the time of their development. And 100 years on the shelf is plenty of time during which everything from further and deeper deposition to erosion of the sediment can happen.

15.3.3 Two-Step Models for Combined Complex Transport/Reaction Processes

The main problem encountered in modeling combinations of advective/dispersive and/or diffusive transport, on the one hand, and any (bio)geochemical reaction, on the other hand, is that at least two totally different processes interact simultaneously on the same object:

Physical transport including diffusion, advection and dispersion, when reactions are absent, is one part of the problem. In their entirety, these processes are quantitatively well understood in model concepts. They are also applicable, without raising principle problems, in analytical and numerical solutions to the general partial differential equations of material transport.

Geochemical and (bio)geochemical processes which are independent of transport processes present the other part of the problem. Here as well, there is a number of far advanced model concepts. The models belonging to the PHREEQE or PHREEQC - type may be referred to in this respect (cf. Section 15.1.1 and 15.1.2). Other fields are object of the various chapters in this book.

First, attempts were made to develop models that could accomplish the coupling of both process groups in one single, either analytical or numerical procedure, although these often bore strong limitations for the application to geochemical reactions. Attempts now more often foresee solutions in two steps. This group of methods is referred to either as "operator splitting", or as the "two-step method". Boudreau (1997) mentions this procedure only briefly at the close of his book and describes it as 'an apparently crazy idea that works rather well in practice'. The first versions of such models, which couple physical transport to geochemical reactions in groundwater are already more than 20 years old (e.g. Schulz and Reardon 1983). Application examples for the 'two-step method' in modeling diagenetic processes in marine sediments over the recent years were published by Hamer and Sieger (1994), Van Cappellen and Wang (1995), Wang and Van Cappellen (1996), Hensen et al. (1997), Sieger (1993), Landenberger et al. (1997), Landenberger (1998), Adler et al. (2000a), Adler et al. (2001), Wenzhöfer et al. (2001), Pfeifer et al. (2002), Haese et al. (2003), Hensen et al. (2003).

The model CoTReM (**Co**lumn **T**ransport and **Re**action **M**odel) (Adler et al. 2000b) is primarily designed for its application to complex early diagenetic reactions in marine sediments. In the one-dimensional transport part of the model (as a continuance of the model DISPER by Flühler and Jury 1983) the model's territory is divided up into a variable number of REVs (representative elementary volumes). These REVs may differ in

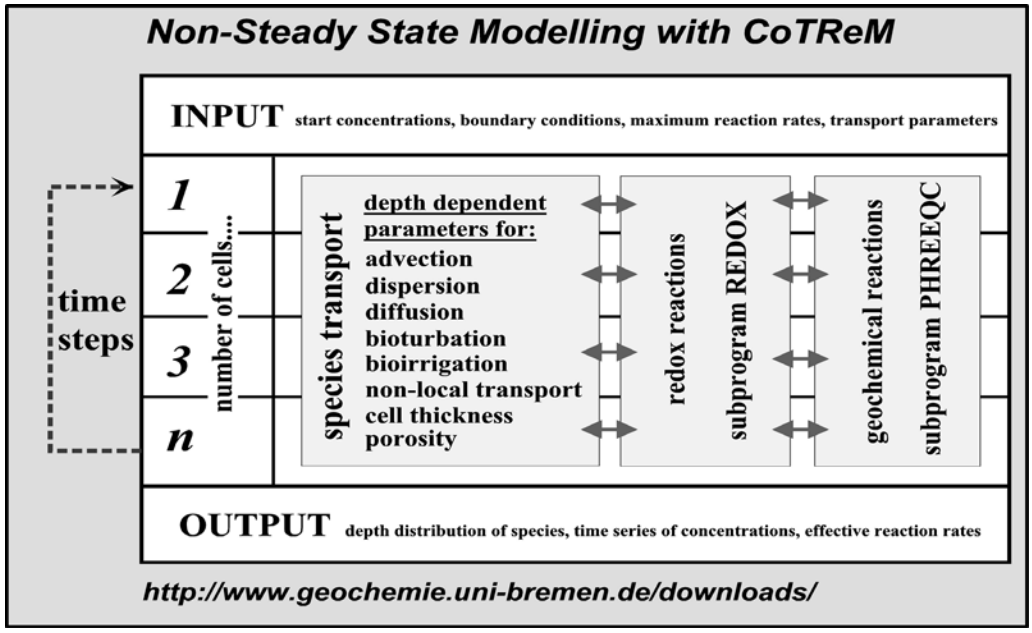

Fig. 15.15 Functional principle of the CoTReM model in the simulation of early diagenetic processes in sediments. The time series of (bio)geochemical reactions and material transport are alternately simulated in a two-step procedure. PHREEQC is used as a subroutine for geochemical reactions. CoTReM, including instructions and exemplary data, can be downloaded from the internet site indicated.

length, porosity, and in their dispersion and diffusion properties.

The time to be modeled is subdivided into a number of time steps. First, a numerical solution is used to solve the partial differential equation of transport (including adsorption and desorption) with respect to all substances under study. Afterwards, the geochemical processes in each REV are modeled independent of transport processes. For this step, CoTReM runs a subroutine called REDOX, as well as the geochemical equilibrium and reaction model PHREEQC. The next time step is processed by starting again with the physical transport, followed by the geochemical reactions etc., until the pre-determined operating time is completed. The structural principle of the model CoTReM is outlined in Figure 15.15.

The latest version of CoTReM together with a program description and data files of some examples is available at the internet web page, mentioned above.

An example which was published by Pfeifer et al. (2002) illustrates very clearly the functions provided by CoTReM. The authors processed a sediment core obtained from the equatorial upwelling area off the coast of West Africa (Location GeoB4906, water depth 1251 m). The left diagram in Figure 15.16 shows the concentration profiles of oxygen, nitrate, manganese, iron, and sulfate in the upper six centimeters of the core, along with the results of the model calculation made with CoTReM. The concentrations of ammonia and calcium, the pH and pCO_2 were also measured and included into the calculation (not shown). The following processes had to be included into the modeling procedure:

- Oxidation of organic matter by oxygen
- Oxidation of organic matter by nitrate
- Oxidation organic matter by iron oxide or iron hydroxide
- Oxidation of organic matter by sulfate
- Re-oxidation of dissolved divalent manganese by oxygen
- Re-oxidation of dissolved divalent iron by nitrate
- Re-oxidation of dissolved divalent iron by manganese oxide
- Dissolution/precipitation of iron sulfide and calcite

The adjustment of all reactions to the measured profiles was made by the depth-dependent turnover rates or reaction kinetics of the indivi-

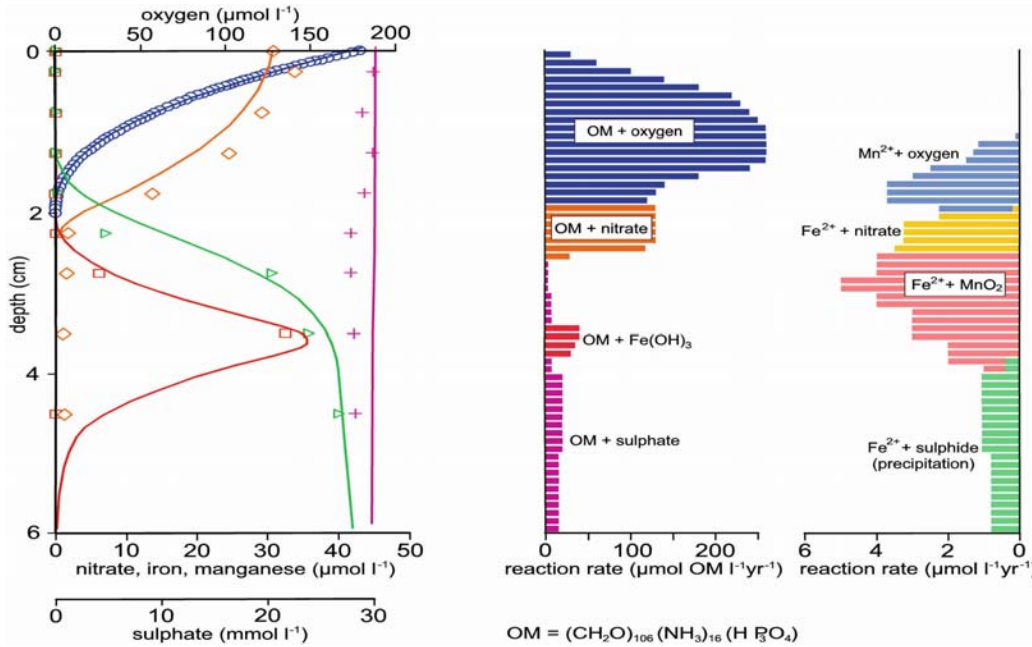

Fig. 15.16 Measurements and results of a model calculation performed with CoTReM applying to the upper centimeters of a sediment core from equatorial West Africa (GeoB4906, 1251 m water depth) (after Pfeifer et al. 2002). The symbols in the left diagram represent measured values of pore-water concentrations (circles: oxygen, diamonds: nitrate, triangles: manganese, squares: iron, crosses: sulfate). The unbroken lines denote the concentrations calculated by the model. The right diagram illustrates the assumed (bio)geochemical reactions which take place in various depths and display dissimilar turnover rates. (OM: Organic matter).

dual processes. In this regard CoTReM permits modeling to start with the maximum turnover rates, which the program subsequently reduces to realistic values. As some of the reactions interact with each other, the adjustment of the model to the concentration profiles of the single parameters often involves a laborious process of step-by-step procedure that requires a repeated subsequent correction of the depth-related turnover rates. However, there is no other way which could be better and especially easier to understand the complex interacting system of early diagenesis in the sediment. The right diagram in Figure 15.16 shows the depth distribution of the turnover rates, which were ultimately necessary for adjustment. Hence they also provide the basis for a quantitative understanding of all processes that are relevant to this sediment.

An also very versatile program designed for modeling the essential processes in early diagenesis originates from Wang and Van Capellen (1996), or Van Cappellen and Wang (1995). This model STEADYSED1 can be obtained from the authors as 'public domain software' and enables the operator to change and adjust all essential sets of data to a particular problem. Yet, one can also select and apply far more unreasonable combinations than reasonable ones - which is in the nature of the model considering the complexity the model offers. The agreeable 'learning by playing' which is typical for so many simple models, turns out to be not so easy after all.

The model uses the following physical data: the sedimentation rate for solid phase advection, temperature for correcting diffusion, porosity and the derived formation factor. A description of bioturbation is obtained by utilizing a mixture-related coefficient, comparable to the diffusion coefficient. An indication of depth informs how far below the sediment surface bioturbation will be effective.

Constant concentrations are assumed for the following components in bottom water: O_2, NO_3^-, SO_4^{2-}, Mn^{2+}, Fe^{2+}, NH_4^+, salinity, alkalinity and pH-value. As the model STEADYSED1 exclusively tolerates steady state situations, this assumption naturally requires constant concentrations in bottom water as a prerequisite.

As for the solid phase of sediment, the input of iron and manganese oxides, the amount of organic substance, and the C:N:P ratio of the organic substance are used. The diagenetic decomposition of the organic substance mediated by the electron acceptors oxygen, nitrate, manganese and iron oxides, sulfate, all the way to methane fermentation, is simulated according to the reactions published by Froelich et al. (1979). However, the user may also select the C:N:P ratio of the organic substance. The re-oxidation of iron sulfides, and manganese sulfides, or of methane is

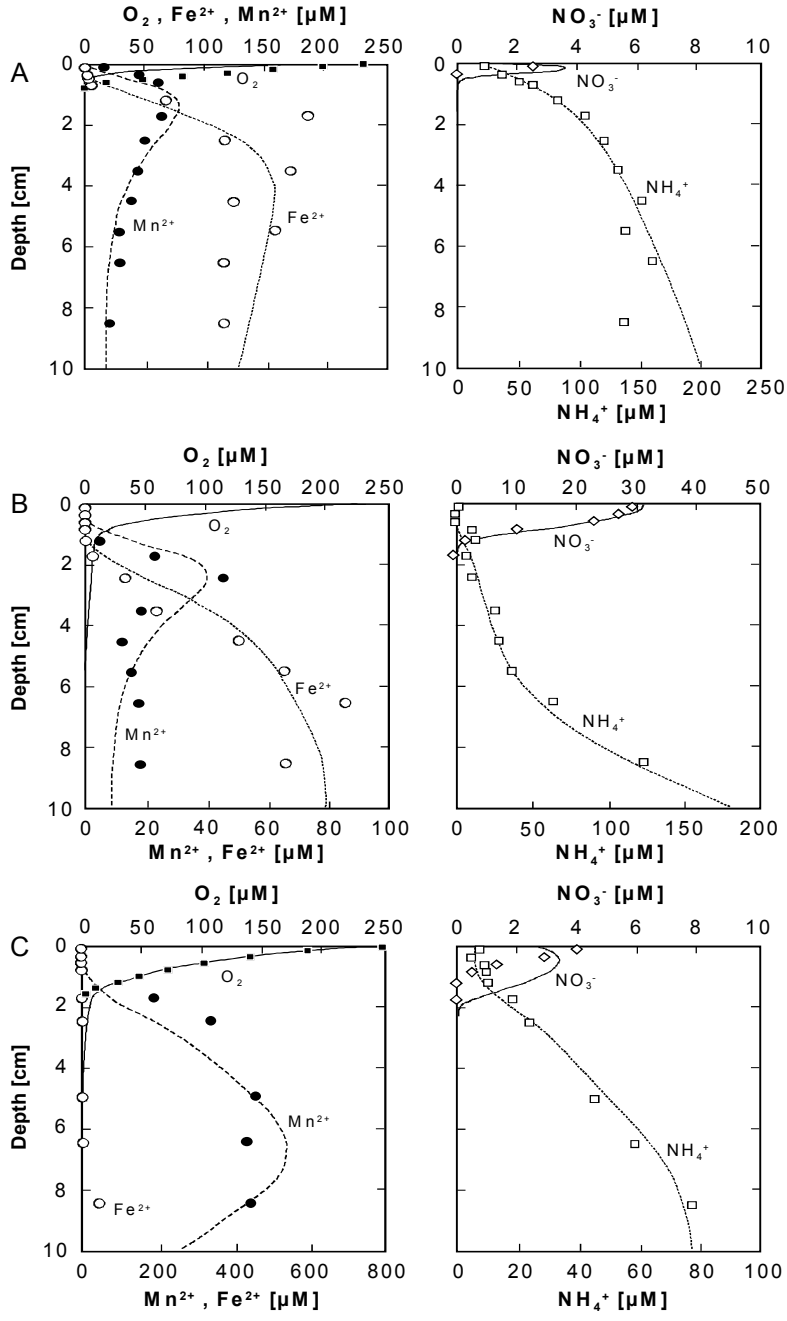

Fig. 15.17 Concentration profiles in pore water of three examples from marine sediments. Data represented by symbols were taken from Canfield et al. (1993 a,b), whereas the curves demonstrate the respective simulations carried out with the model STEADYSED1 by Wang and Van Cappellen (1996).

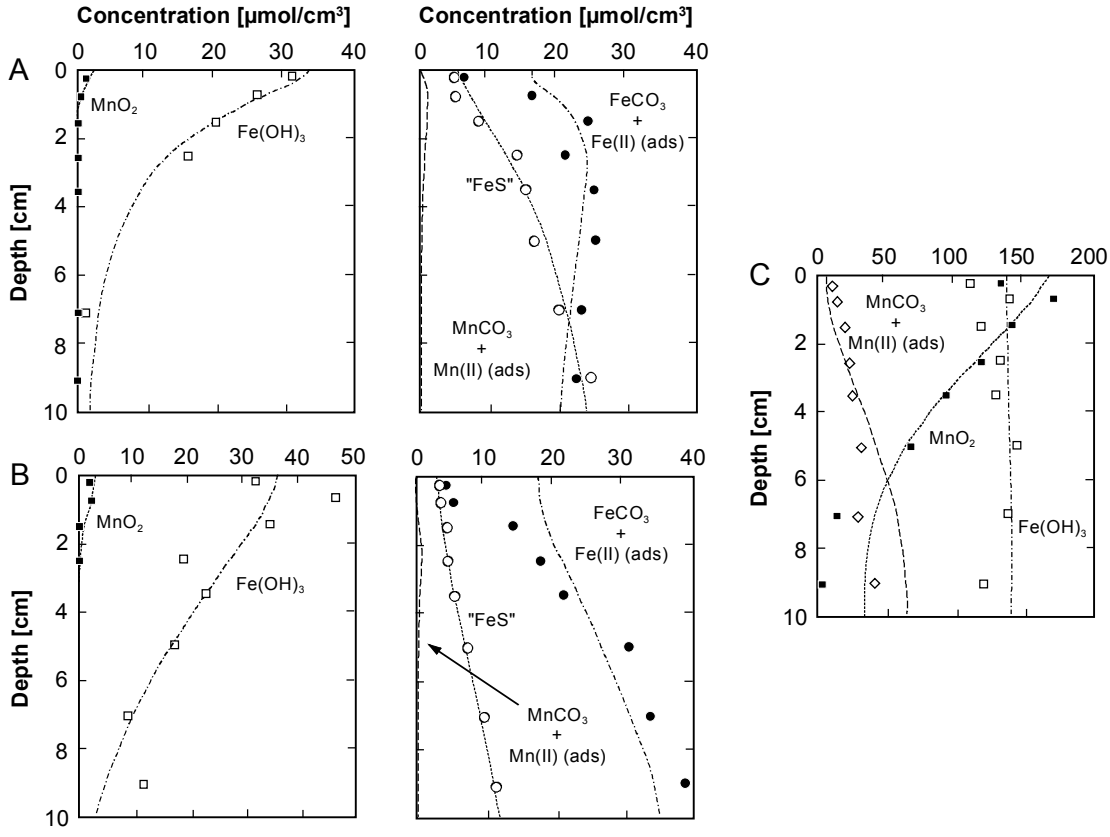

Fig. 15.18 Concentration profiles of iron and manganese solid phases in sediments derived from three marine examples. Data represented by symbols were taken from Canfield et al. (1993 a,b), whereas the curves demonstrate the respective simulations carried out with the model STEADYSED1 by Wang and Van Cappellen (1996).

preferably performed as 'secondary redox reactions'. Moreover, the adsorption of ammonium, and the precipitation/dissolution of iron carbonate, manganese carbonate, and iron sulfide can be included. For all these reactions, the analyst is able and *required* to select the adequate rates.

This is where the general problems in applying such models occur: with all the parameters and boundary conditions that need to be set, there will be so many 'buttons' and control options ultimately allowing for almost any kind of modeling of the measured data. Only if so many examples are available as Wang and Van Cappellen (1996) found in the data of Canfield et al. (1993a, b) based on measurements, will it be possible to come to substantial and reasonable results. Figure 15.17 shows concentration profiles for O_2, NO_3^-, NH_4^+, Mn^{2+}, Fe^{2+} measured in the pore water of three cores. Figure 15.18 demonstrates the solid phase concentration profiles of Fe- and Mn participating in the reactions.

If one compares the two model programs CoTReM by Adler et al. (2000b), on the one hand, and the model STEADYSED1 published by Wang and Van Cappellen (1996) on the other, the following aspects need to be emphasized:

- Both models have been made freely available by the respective authors as public domain software and hence can be used by everyone.
- Both models are not easy to operate and require at least some background knowledge in modeling procedures and early diagenetic reactions.
- Both models simulate the complex situation of combining diffusive, advective and bioturbational transports in pore water and in the solid phase. They contain the various reactions of early diagenesis and require a large number of reliable measurements. Otherwise, too many degrees of freedom would remain.

- Both models contain the possibility to simulate bioirrigation; STEADYSED1 generally treats bioirrigation and bioturbation with much more thoroughness and reliability.
- STEADYSED1 is quite limited as far as its chemical processes are concerned (absence of real activities in the pore water, and hence only apparent equilibrium constants, complex species are not included). However, it contains all the essential processes currently known. CoTReM is much more flexible owing to the utilization of PHREEQC (Parkhurst 1995) as a subroutine, yet it requires proportionally more information.
- The model CoTReM works with Fick's Second Law of Diffusion and thus permits the calculation of any possible, especially non-steady state situations. STEADYSED1 can only be applied to calculate steady state situations which accordingly demand the existence of steady state boundary conditions.

15.4 Bioturbation and Bioirrigation in Combined Models

Bioturbation is normally modeled by applying a bio-diffusion coefficient to the pore water fraction *and* the solid phase. This means that a bio-diffusion in the solid phase will be simulated with the same model concept which is applied in the form of Fick's laws to the dissolved constituents in pore water. Under the assumption of a given steady state (e.g. STEADYSED1), this requires that a sufficient length of time is studied which allows the macroorganisms contributing to bioturbation to display activity all over and as many times as appears necessary. Only then will each part of the solid phase be turned over often enough in the statistical balance, hence providing a workable model concept. As for cases of non-steady state and short observation periods the model concept actually cannot be considered as valid.

Figure 15.19 shows, in one exemplary model calculation carried out with STEADYSED1, the conversion rates of iron and manganese in the upper sediment zone and their exchange with the supernatant bottom water layer. It is evident that the amounts of iron which ultima-

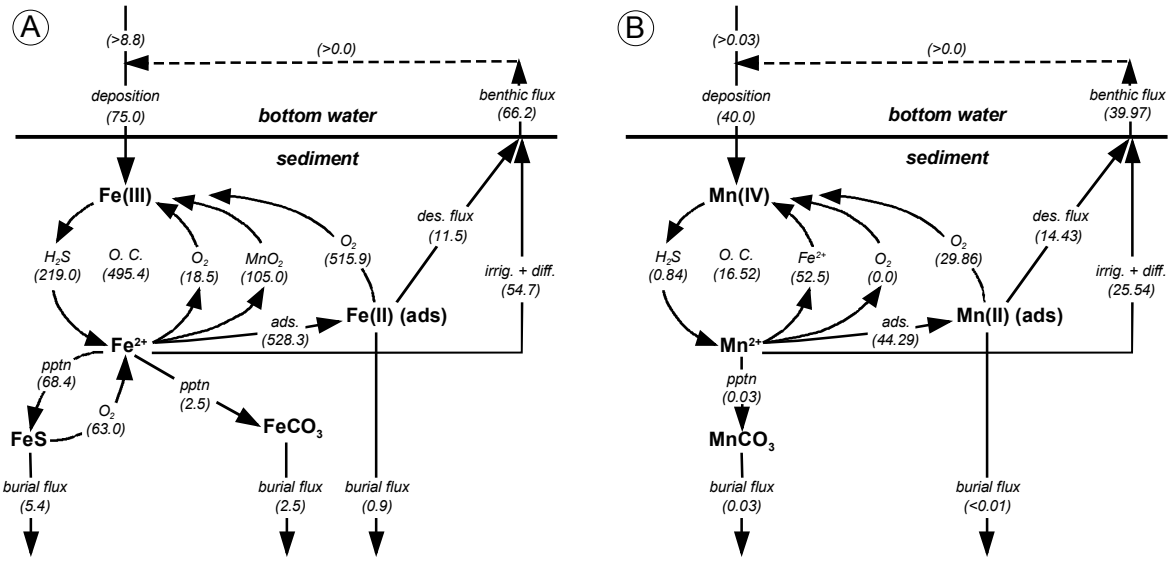

Fig. 15.19 Iron and manganese fluxes in superficial marine sediments and bottom water, as obtained from calculations using the model STEADYSED1 by Wang and Van Cappellen (1996). Here, it is significant that bioturbation and bioirrigation were included in the task.

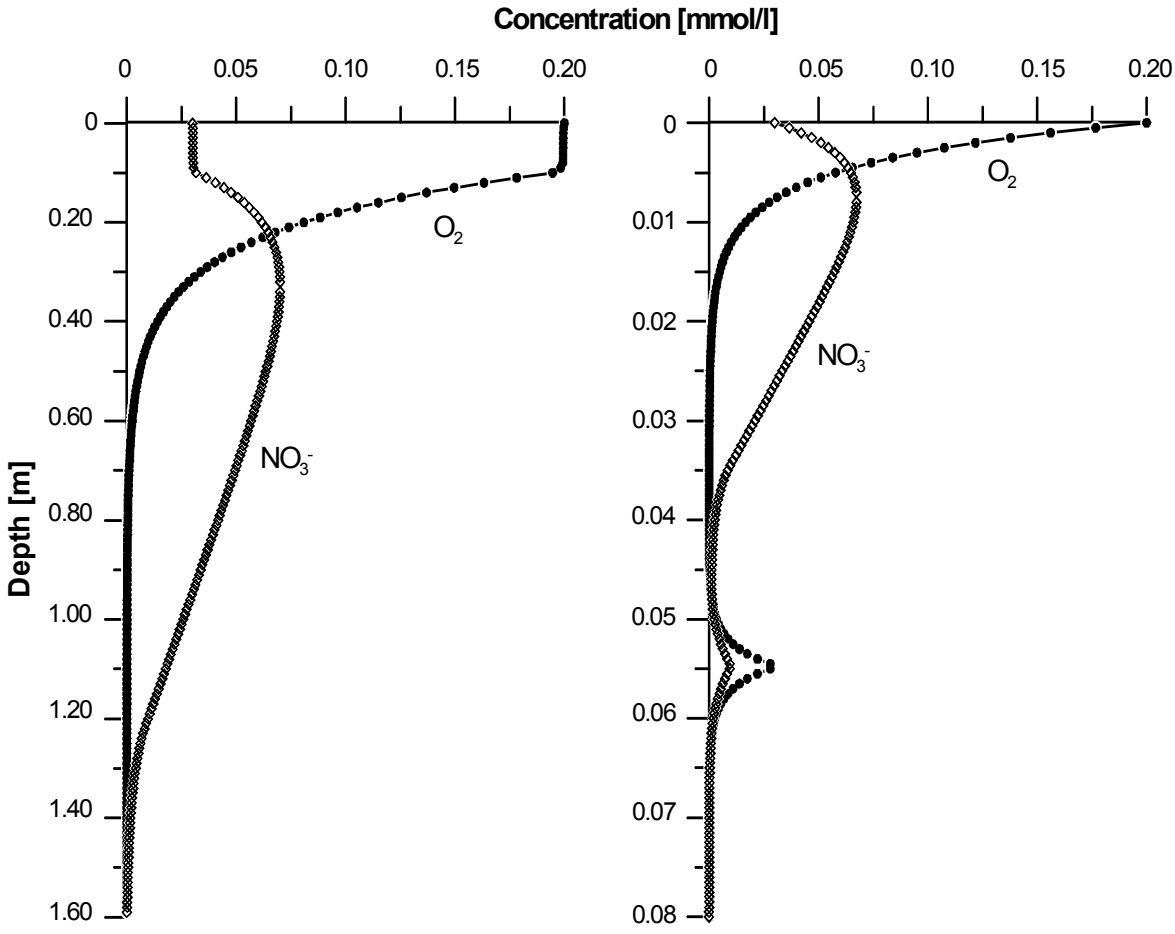

Fig. 15.20 Left: Oxygen and nitrate profiles influenced by bioirrigation within the upper 10 cm as modeled with an Excel® spreadsheet according to the 'Press F9 method'. The simulation was performed on the basis of anticipating a partial coupling of pore water to the concentrations prevalent in bottom water in the upper 10 cm of the sediment. Right: Here, a quantity of bottom water was continually added in a specific depth. The result is related to the measurement shown in Figure 3.24 after Glud et al. (1994).

tely become deposited in the sediment (burial flux) as FeS, $FeCO_3$, or in an adsorbed state, are essentially smaller than the amounts undergoing conversions in the upper parts of the sediment and which have therefore undergone redox processes several times before. The lower part of Figure 15.19 demonstrates the corresponding turnovers of manganese with again quite specific ratios between the burial flux, conversion rates in the upper sediment zone, and exchange with the bottom water.

The simulation of bioirrigation is much more difficult, a circumstance which pertains to its nature, since the process, endowed with great inhomogeneity and strong dependence on the organism under study, combines bottom water with pore water at the particular depths concerned. How this combination becomes effective in any one particular case, and to which degree it also influences the pore water not involved directly, naturally depends on the macroorganisms presently responsible for the effect. Thus, the process actually eludes a generalized solution and should be treated individually for each special case. To this end, workable models are not available in sufficient number, neither are there any adequately applicable modeling techniques at hand.

In Figure 15.20, and by using the 'Press-F9-method' described in Section 15.3.1, two steady states displaying bioirrigation have been calculated. The case shown on the left-hand side

anticipates an upper sediment zone continually influenced by bioirrigation, whereas the case shown on the right merely assumes surface coupling in a specific depth - e.g., by the effect of a particular worm-hole. The result may be compared with the measurements conducted by Glud et al. (1994) and shown in Figure 3.32. Just as Wang and Van Cappellen (1994) have described it in one application of the model STEADYSED1, the situation here is that bioirrigation conveys nitrate into the sediment, whereas, at the same time, molecular diffusion transports nitrate from the sediment back into the bottom water. This results from the fact that both processes are coupled to the bottom water layer in different depths of the sediment. In the case of diffusion, these are the superficial nitrate-rich zones, whereas in the case of bioirrigation, the deeper situated zones are effective, which contain only small amounts of nitrate.

Ultimately, all these agreements between the measured profile and the resultant model are not really significant since they merely represent a direct application of the model concept of bioirrigation, i.e., the pore water input conducted from the bottom water at a certain depth in the sediment. Yet, these models are only interesting inasmuch as the non-diffusive transport between sediment and bottom water results from them. These are exemplified for iron and manganese in Figure 15.19, calculated with a similar model concept using the program STEADYSED1. It should be kept in mind that these calculations are only workable to the point as they comply to a rather simplified model concept and to a stationary situation anticipated not only in the 'Press F9 method' but in STEADYSED1 as well. Only by conducting measurements of the material fluxes *in-situ* at very dissimilar locations, and after repeated comparisons with the adequate models have been made, will the previous model concepts and the calculated fluxes ever become verified in the future.

Acknowledgements

This is contribution No 0337 of the Research Center Ocean Margins (RCOM) which is financed by the Deutsche Forschungsgemeinschaft (DFG) at Bremen University, Germany.

15.5 Problems

Problem 1

Table 15.1 shows an analysis of ocean water made by Nordstrom et al. (1979). A condition of oversaturation of the minerals calcite (SI = 0.76) and dolomite (SI = 2.4) at a measured pH value of 8.22 has been calculated for this analysis with the model PHREEQC (see also Table 15.3). What pH is to be expected if we calculate the saturation state of both minerals in this ocean water sample with PHREEQC under the condition of log pCO_2 = –3.47 ?

Problem 2

At which pCO_2 would the mineral calcite in the ocean water sample in Table 15.1 (Nordstrom et al., 1979) be saturated if a pH value of 8.22 had been measured ? How could this pCO_2 which is markedly below the value of the atmospheric be explained ?

Problem 3

What penetration depth of oxygen would you expect in a sediment, if the removal of oxygen can be described in terms of a half-life of 5 days? Sediments have a temperature of 10°C. Their porosity is at 70 percent. For the diffusion coefficients use Tables 3.1 and 3.2. The bottom water shall have an oxygen concentration of 200 µmol l^{-1}. Use an oxygen concentration less than 1 µmol l^{-1} as "zero".

Problem 4

A different sulfate concentration gradient is measured above the sulfate-methane transition zone than underneath the methane zone. How could this be explained, despite the fact that sulfate and methane react with each other in a ratio of 1:1 ?

References

Adler M., Hensen C., Kasten S. and Schulz H.D. (2000a) Computer simulation of deep sulfate reduction in sediments of the Amazon Fan. Internat. Journal of Earth Sciences, 88, pp. 641-654

Adler M., Hensen C. and Schulz H.D. (2000b) CoTReM – Column Transport and Reaction Model, Version 2.3, User Guide. http://www.geochemie.uni-bremen.de/downloads/cotrem/index.htm, 59 pp.

Adler M., Hensen C., Wenzhöfer F., Pfeifer K. and Schulz H.D. (2001) Modeling of calcite dissolution by oxic respiration in supralysoclinal deep-sea sediments. Marine Geology, 177, pp. 167-189

Ball J.W. & Nordstrom D.K. (1991) WATEQ4F - User´s manual with revised thermodynamic data base and test cases for calculating speciation of major, trace and redox elements in natural waters. US Geol. Surv., Open-File Report 90-129, 185 pp

Berner R.A. (1980) Early Diagenesis: A Theoretical Approach. Princeton Series in Geochemistry, Princeton University Press, 241 pp

Bleil U. and participants (1994) Report and preliminary results of *Meteor* cruise M29/2 Montevideo-Rio de Janeiro, 15.7.-08.08.1994, Vol. 59, Fachbereich Geowissenschaften, Universität Bremen, 153 pp.

Boudreau B.P. (1997) Diagenetic Models and Their Implementation: Modelling Transport and Reactions in Aquatic Sediments. Springer-Verlag, Berlin, Heidelberg, New York, 414 pp.

Canfield D.E., Thamdrup B. and Hansen J.W. (1993a) The anaerobic degradation of organic matter in Danish coastal sediments: Iron reduction, manganese reduction, and sulfate reduction. Geochim. Cosmochim. Acta 57, pp. 3867-3883

Canfield D.E., Jørgensen B.B., Fossing H., Glud R., Gundersen J., Ramsing N.B., Thamdrup B., Hansen J.W., Nielsen L.P., Hall P.O.J. (1993b) Pathways of organic carbon oxidation in three continental margin sediments. Mar. Geol. 113, pp. 27-40

Froelich P.N., Klinkhammer G.P., Bender M.L., Luedtke N.A., Heath G.R., Cullen D., Dauphin P., Hammond D., Hartman B. (1979) Early oxidation of organic matter in pelagic sediments of eastern equatorial Atlantic: suboxic diagenesis. Geochim. Cosmochim. Acta, 43, pp. 1075-1090

Flühler H. and Jury W.A. (1983) Estimating solute transport using nonlinear, rate dependent, two-site-adsorption models. Microfiche, Eidg. Anst. forstl. Versuchswesen, 245, Zürich, 48 pp.

Garrels R.M. (1960) Mineral Equilibria at Low Temperature and Pressure. New York (Harper), 254 pp.

Garrels R.M. and Christ Ch.L. (1965) Solutions, Minerals and Equilibria. New York-Evanston-London (Harper & Row)-Tokyo (Weatherhill), 450 pp.

Glasby G.P. and Schulz H.D. (1999) E_H, pH diagrams for Mn, Fe, Co, Ni, Cu and As under seawater conditions: Application of two new types of E_H, pH diagrams to the study of specific problems in marine geochemistry. Aquatic Geochemistry, 5, pp. 227-248

Glud R.H., Gundersen J.K., Jørgensen B.B., Revsbech N.P., Schulz H.D. (1994) Diffusive and total oxygen uptake of deep-sea sediments in the eastern South Atlantic Ocean: in situ and laboratory measurements. Deep-Sea Res., 41, pp. 1767-1788

Haese R.R., Meile C., Van Cappellen P., De Lange G.J. (2003) Carbon geochemistry of cold seeps: Methane fluxes and transformation in sediments from Kazan mud volcano, eastern Mediterranean Sea. Earth and Planetary Science Letters, 212, pp. 361-375

Hamer K. und Sieger R. (1994) Anwendung des Modells CoTAM zur Simulation von Stofftransport und geochemischen Reaktionen. Verlag Ernst & Sohn, Berlin, 186 pp.

Hensen C., Landenberger H., Zabel M., Gundersen J.K., Glud R.N. and Schulz H.D. (1997) Simulation of early diagenetic processes in continental slope sediments off Southwest Africa: The computer model CoTAM tested. Marine Geology, 144, pp. 191-210

Hensen C., Zabel M., Pfeifer K., Schwenk T., Kasten S., Riedinger N., Schulz H.D. and Boetius, A. (2003) Control of sulfate pore-water profiles by sedimentary events and the significance of anaerobic oxidation of methane for the burial of sulfur in marine sediments. Geochimica and Cosmochimica Acta, 67, pp. 2631-2647

Kharaka Y.K., Gunter W.D., Aggarwal P.K., Perkins E.H. and DeBraal J.D. (1988) SOLMINEQ88: a computer program for geochemical Modeling of water-rock-interactions. US Geol. Surv., Water-Resources Investigations Report 88-4227, 207 pp.

Kinzelbach W. (1986) Groundwater Modelling - An Introduction with Sample Programs in BASIC. Elsevier, Amsterdam - Oxford - New York - Tokyo, 333 pp.

Landenberger H., Hensen C., Zabel M. und Schulz H.D. (1997) Softwareentwicklung zur computergestützten Simulation frühdiagenetischer Prozesse in marinen Sedimenten. Ztschr. dt. geol. Ges., 148, pp. 447-455

Landenberger H. (1998) CoTReM, ein Multi-Komponenten Transport- und Reaktions-Modell. Berichte, Fachbereich Geowissenschaften, Univ. Bremen, 110, 142 pp.

Niewöhner C., Hensen C., Kasten S., Zabel M., Schulz H.D. (1998) Deep sulfate reduction completely mediated by anaerobic methane oxidation in the upwelling area off Namibia. Geochim. Cosmochim. Acta, 62, pp. 455-464

Nordstrom D.K., Plummer L.N., Wigley T.M.L., Wolery T.J., Ball J.W., Jenne E.A., Basset R.L., Crerar D.A., Florence T.M., Fritz B., Hoffman M., Holdren G.R., Jr., Lafon G.M., Mattigod S.V., McDuff R.E., Morel F., Reddy M.M., Sposito G. and Thrailkill J. (1979) A comparison of computerized chemical models for equilibrium calculations in aqueous systems: in Chemical Modeling in aqueous systems, speciation, sorption, solubility, and kinetics. Jenne, E.A., ed. Series 93, American Chemical Society, pp. 857-892

Parkhurst D.L. (1995) User´s guide to PHREEQC: a computer model for speciation, reaction-path, advective-transport, and inverse geochemical calculations. US Geol. Surv., Water-Resources Investigations Report 95-4227, 143 pp.

Parkhurst D.L. and Appelo C.A.J (1999) User´s guide to PHREEQC (Version 2): A computer program for speciation, batch-reaction, one-dimensional transport, and inverse geochemical calculations. US Geol. Surv., Water-Resources Investigations Report 99-4259, 312 pp.

Parkhurst D.L., Thorstenson D.C. and Plummer L.N. (1980) PHREEQE - a computer program for geochemical calculations. US Geol. Surv., Water-Resources Invest. 80-96, 219 pp.

Pfeifer K., Hensen C., Adler M., Wenzhöfer F., Weber B. and Schulz H.D. (2002) Modeling of subsurface calcite dissolution, including the respiration and reoxidation processes of marine sediments in the region of equatorial upwelling off Gabon. Geochimica and Cosmochimica Acta, 66, pp. 4247-4259

Plummer L.N., Jones B.F. and Truesdell A.H. (1976) WATEQF - a fortran IV version of WATEQ, a computer program fpr calculating chemical equilibrium of natural waters. US Geol. Surv., Water-Resources Invest. 76-13, 615 pp.

Redfield, A.C., 1958. The biological control of chemical factors in the environment. Am. Sci., 46: 206 226.

Schulz H.D. (2004) Auswertung von Markierungsversuchen. In Käss W. (Ed.) Geohydrologische Markierungstechnik, Lehrbuch der Hydrogeologie Bd.9, S.347-356, Borntraeger-Verlag, Berlin, Stuttgart.

Schulz H.N. and Schulz H.D. (2005) Large Sulfur Bacteria and the Formation of Phosphorite. Science, 307, pp. 416-418

Schulz H.D. and Reardon E.J. (1983) A combined mixing cell/analytical model to describe two-dimensional reactive solute transport for unidirectional groundwater flow. Water Resour. Res, 19, pp. 493-502

Schulz H.D., Dahmke A., Schinzel U., Wallmann K., Zabel M. (1994) Early diagenetic processes, fluxes, and reaction rates in sediments of the South Atlantic. Geochim. Cosmochim. Acta, 59, pp. 2041-2060

Sieger R. (1993) Modellierung des Stofftransports in porösen Medien unter Ankopplung kinetisch gesteuerter Sorptions- und Redoxprozesse sowie thermodynamischer Gleichgewichte. Berichte, Fachbereich Geowissenschaften, Univ. Bremen, 110, 142 pp.

Truesdell A.H. and Jones B.F. (1974) WATEQ, a computer program for calculating chemical equilibria on natural waters.- Jour. Research US Geol. Surv., Washington D.C., 2, pp. 233-248

Van Cappellen P. and Wang Y. (1995) STEADYSED1: A Steady-State Reaction-Transport Model for C, N, S, O, Fe and Mn in Surface Sediments. Version 1.0 User´s Manual, Georgia Inst. Technol., 40 pp.

Van Cappellen P., Wang Y. (1996) Cycling of iron and manganese in surface sediments: a general theory for the coupled transport and reaction of carbon, oxygen, nitrogen, sulfur, iron, and manganese. Amer. Journal of Science, 296, pp. 197-243

Van Cappellen P. and Gaillard J.-F. (1996) Biogeochemical Dynamics in Aquatic Sediments. In: Lichtner P.C., Steefel C.I. and Oelkers E.H. (eds.) Reviews in Mineralogy, Vol. 34: Reactive Transport in Porous Media, The Mineralogical Society of America, Washington DC., pp. 335-376

Wang Y. and Van Cappellen P. (1996) A multicomponent reactive transport model of early diagenesis: Application to redox cycling in coastal marine sediments. Geochim. Cosmochim. Acta, 60, pp. 2993-3014

Wenzhöfer F., Adler M., Kohls O., Hensen C., Strotmann B., Boehme S. and Schulz H.D. (2001) Calcite dissolution driven by benthic mineralization in the deep-sea: In situ measurements of Ca^{2+}, pH, pCO_2 and O_2. Geochimica et Cosmochimica Acta, 65, pp. 2677-2690

Wolery T.J. (1993) EQ 3/6, A Software Package for Geochemical Modeling of Aqueous Systems. Lawrence Livermore National Laboratory, California, 247 pp.

Zabel M. and Schulz H.D. (2001) Importance of submarine landslides for non steady state conditions in pore water systems – lower Zaire (Congo) deep-sea fan. Marine Geology, 176, pp. 87-99